Chapter 7

Preparation and characterization of specific adsorbents for Mercury

Outline:

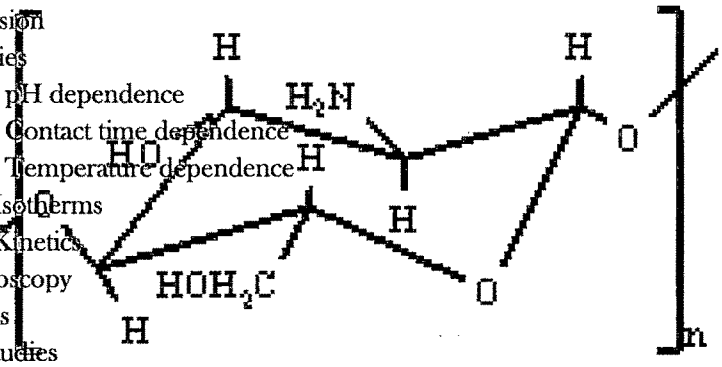

7.1. Introduction

Agricultural waste materials as we have seen in chapter 1 and 2 are usually composed of lignin and cellulose as the main constituents. Other components are hemicellulose, extractives, lipids, proteins, simple sugars, starches, water, hydrocarbons, ash and many more compounds that contain a variety of functional groups present in the binding process. Cellulose is a crystalline homo-polymer of glucose with β1→ 4 glycosidic linkage and intra-molecular and intermolecular hydrogen bonds [1, 2]. Hemicellulose is a heteropolymer of mainly xylose with β1→ 4,4 glycosidic linkage with other substances of acetyl feruoyl and glycouronyl groups [3]. Lignin is three dimensional polymer of aromatic compounds covalently linked with xylans in hardwoods and galactoglucomannans in softwoods [4, 5]. The functional groups present in biomass molecules acetamido groups, carbonyl, phenolic, structural polysaccharides, amido, amino, sulphydryl carboxyl groups alcohols and esters [6, 7]. These groups have the affinity for metal complexation. Some biosorbents are non-selective and bind to a wide range of heavy metals with no specific priority, whereas others are specific for certain types of metals depending upon their chemical composition.

Similar observations of non selectivity or selectivity for a group of metals has been made by us with the adsorbents under study namely PSP, APSP, SAPSP, PAPSP, 9AAC and MPSP. Surface modification has become a common technique in providing a material with desirable functional properties one of which is selectivity.

Chitosan is a linear polysaccharide composed of β (1→4) linked 2-amino-2-deoxy-D-glucose and 2-acetamido-2-deoxy-D-glucose units. Chitosan is soluble in all organic and mineral acids and has reduced diffusivity of sorbate due to its low porosity and high crystallinity. It is biodegradable and has gelling ability. Chitosan, has widely been studied as an adsorbent with good metal-chelating properties for the removal of various heavy metal ions from water or wastewater [7, 11-15]. It is generally known that the amine groups in chitosan are the main binding sites for the heavy metal ions, but the amine groups do not show specific selectivity toward individual heavy metal species [16]. In recent years, surface modification has become a popular method for providing a material with desirable properties for practical applications, and many methods of surface modification have been developed [17,18]. Thanks to its amino groups,

chitosan is reactive towards many chemicals: this results in a number of chitosan derivatives having a wide range of uses, and in particular as transition metal chelates [10-17].

Chitosan and its derivatives have been used for removal of metal ions from waste water [34-44]. The suitability of chitosan and cross-linked chitosan have been studied for adsorption of mercury [37, 38]. Elemental mercury removal on chitosan, iodine (bromide) or sulfuric acid modified chitosan has been studied [36]. Limited reports have been found in the literature on removal of methyl mercury and phenyl mercury using chitosan as an adsorbent. Methyl mercury adsorption has been studied using chitosan as an adsorbent in a column [34]. Several investigations were done to modify chitosan to facilitate mass transfer and to expose the binding sites to enhance the adsorption capacity [45]. Chitosan and chitosan grafted polyacrylamide beads, thiol modified chitosan have been reported for the adsorption of inorganic mercury [35, 46].

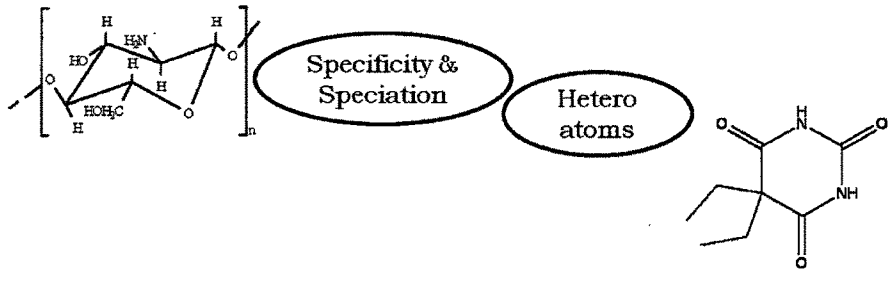

Many reviews are available in literature regarding adsorption of mercury onto chitosan [18-20], Table 7.1 also describes the reports available in literature for adsorption of mercury by different chitosan derivatives along with their maximum adsorption capacities.

Table 7.1. Chitosan based adsorbents with their adsorption capacity and adsorption parameters

Adsorbent	Metal	Operating Conditions		Max. Ads. Cap. (mg/g)	References
		Temp.	pH		
Natural chitosan	Hg(II)	313K	5.0	16.1	[21]
	Hg(II)	313K	6.0	25.3	
	Hg(II)	313K	7.0	24.7	
Glutraladehyde cross linked chitosan	Hg(II)	313K	5	22.3	
	Hg(II)	313K	6	75.5	
	Hg(II)	313K	7	37.5	
Epichlorohydrin cross linked chitosan	Hg(II)	313K	5	16.3	
	Hg(II)	313K	6	30.3	
	Hg(II)	313K	7	22.9	
Ethylenediamine modified chitosan magnetic microspheres	Hg(II)	298K	5	2.69	[22]
	Hg(II)	308K	5	2.45	
	Hg(II)	318K	5	2.19	
	Hg(II)	328K	5	1.96	
Thiourea-modified magnetic chitosan microspheres	Hg(II)	-	-	625.2	[23]
	Cu(II)	-	-	66.7	
	Ni(II)	-	-	15.3	
	Hg(II)	-	-	-	
	Cu(II)	-	-	-	
	Ni(II)	-	-	-	
	Hg(II)	-	-	-	
	Cu(II)	-	-	-	
	Ni(II)	-	-	-	
Chitosan	Cu(II)	333K	2.5	135	[24]
	Hg(II)	-		357	
	Cu(II)	333K	4.5	238	
	Hg(II)	-		454	
Chitosan coated cotton fibres SCCH	Hg(II)	278K	-	0.32	[25]
		278K	-	-	
	Hg(II)	288K	-	0.16	
		288K	-	-	
	Hg(II)	298K	-	0.42	
		298K	-	-	
	Hg(II)	308K	-	0.52	
		308K	-	-	
Chitosan coated cotton fibres RCCH	Hg(II)	278K	-	0.28	
		278K	-		
	Hg(II)	288K	-	0.20	
		288K	-	-	
	Hg(II)	298K	-	0.48	
		298K	-		
	Hg(II)	308K	-	0.38	
		308K	-	-	
Chitosan	Hg(II)	<383K	2	647.4	[26]

Thiocarbomoyl derivative of chitosan S2	Hg(II)	<383K	2	459.5	
	Hg(II)	<383K	5	617.9	
	Hg(II)	<383K	7	1445.0	
	Hg(II)	<383K	7	365.3	
Thiocarbomoyl derivative of chitosan SC2	Hg(II)	<383K	2	459.9	
	Hg(II)	<383K	5	606.9	
	Hg(II)	<383K	7	1271.2	
	Hg(II)	<383K	7	330.7	
Magnetic chitosan resin chemically modified by a Schiff's base cross-linker.	Hg(II)	303K	<7.5	3.060	[27]
	Hg(II)	313K	<7.5	2.688	
	Hg(II)	323K	<7.5	2.520	
	Hg(II)	333K	<7.5	2.214	
Thiol-grafted chitosan beads	Hg(II)	-	2	-	[28]
	Hg(II)	-	4	-	
	Hg(II)	-	4	-	
	Hg(II)	-	5	-	
	Hg(II)	-	7	-	
Aminated chitosan bead prepared through chemical reaction with EDA	Hg(II)	-	4	89	[29]
	Hg(II)	-	5.5	191	
	Hg(II)	-	7	496	
Chemically modified chitosan	Pb(II)	298K	7	-	[30]
	Cu(II)	298K	7	-	
	Cd(II)	298K	7	-	
HDI-crosslinkeddeacetylated Chitin	Cu(II)	323K	7	-	[31]
	Cu(II)	323K	7	-	
TMA-crosslinkeddeacetylated Chitin	Cu(II)	323K	7	-	
	Cu(II)	323K	7	-	
Coarse chitin	-	343K	7	70 ± 8	[32]
	-	343K	7	-	
Fine chitin	-	343K	7	66 ± 8	
	-	343K	7	-	
thiourea-modified chitosan derivative (TMCD)	Hg(II)	299K	-	6.690	[33]
	Hg(II)	309K	-	5.734	
	Hg(II)	319K	-	5.277	
	Hg(II)	329K	-	5.107	

Most of the studies have been done to optimize sorption performances, especially sorption isotherms with some suggesting uptake mechanisms, but little has been done on the identification of the sorption sites and interpretation of the molecular interactions between sorbent and solute by FTIR and mechanistic modeling using potentiometric titrations. The ability of mercury(II) to form a complex with barbital (5,5-diethyl barbituric acid) has been used as the basis for the separation and determination of barbiturates where barbital was treated with

excess mercury(II) to form a chloroform extractable complex [47]. Advantage was taken of the ability of mercury to form a mercury barbital complex for the determination of mercury [48]. This suggested that more detailed study could be done to find the suitability of grafting barbital onto chitosan (BC), cross-linked chitosan using glutaraldehyde (G-Chitosan) and Barbital Glutaraldehyde cross-linked Chitosan (BG-Chitosan) and their use as adsorbents for the removal of inorganic, methyl and phenyl mercury.

Our objectives were

i) Evaluation of C, BC, CL and BCL for the removal of inorganic mercury (Hg^{2+}), methyl (CH_3Hg^{2+}) and phenyl mercury ($PhHg^{2+}$) and optimization of parameters for their maximum removal.

ii) Detailed studies using spectroscopic, potentiometric techniques as well as kinetic and isotherm models to understand the mechanism during the adsorption of different forms of mercury onto C, BC, G-Chitosan and BG-Chitosan.

7.2. Material and method

7.2.1. Sorbent Preparation.

Chitosan flakes (87.6 % deacetylated and molecular weight 5.5 x 10^5 g/mol) from Sigma Aldrich were used to prepare chitosan beads. 1 % (w/w) chitosan solution was prepared by dissolving chitosan flakes in 1 % (w/w) acetic acid solution at room temperature for homogenizing the mixture for 48 hrs. The homogeneous chitosan solution was injected dropwise into 0.41 N NaOH solution for the formation of beads. After the formation of beads it was left overnight in a freezer for hardening (Scheme 7.1). The beads were extensively washed with distilled water until neutral and then used for the preparation of barbital immobilized chitosan and for further experimental studies as adsorbent (C).

For the preparation of barbital immobilized chitosan [BC] (Scheme 7.1), a solution of neutralized beads of chitosan with 1 % sodium barbiturate (dissolved in double distilled water) in the ratio of 1:1 was stirred for 24 h at 50 ^{0}C, filtered, washed with double distilled water until neutral and then left for air drying.

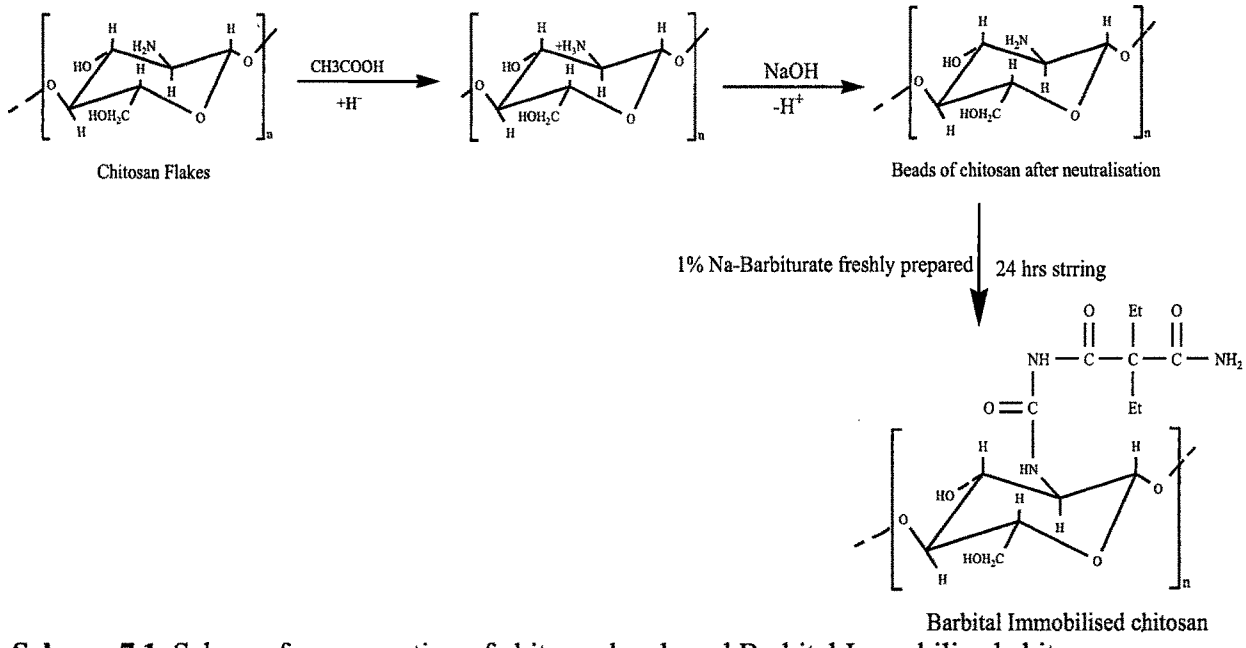

Scheme 7.1. Scheme for preparation of chitosan beads and Barbital Immobilized chitosan

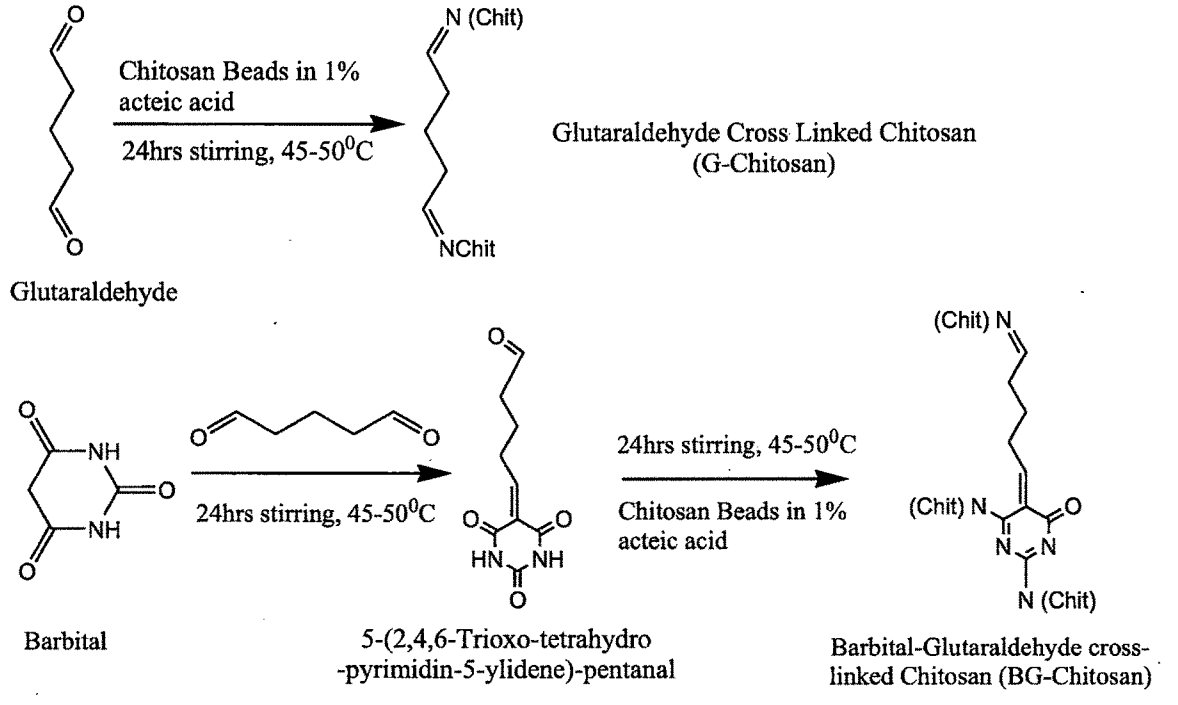

Scheme 7.2. Cross-linking with Glutaraldehyde and Barbital with glutaraldehyde

A 100mL of 0.1% solution of gultaradehyde was added to 100mL of 1% homogenized solution of chitosan in 1% acetic acid and allowed to react for 24hrs at 45-50^{0}C to form an imine [G-

Chitosan] through a Schiff's base reaction between aldehyde ends of glutaraldehyde and amine moieties of Chitosan. Glutaraldehyde cross-linked chitosan (G-Chitosan) was then filtered, washed with double distilled water until neutral and then left for air drying(Scheme 7.2).

Barbital Glutaraldehyde cross-linked Chitosan (BG-Chitosan) was formed by initial condensation of glutaraldehyde and barbiturate moiety followed by cross-linking with chitosan(Scheme 7.2).. A 100mL of 0.1% solution of glutaraldehyde was mixed with 100mL of 0.1% solution of freshly prepared sodium barbiturate and were allowed to react at 45-50^{0}C for 24hrs. This solution was added to 100mL of 1% solution of chitosan in acetic acid and stirred for 24 hrs at 50^{0}C, filtered, washed with double distilled water until neutral and then left for air drying. The barbital glutaraldehyde condensation product (5-(2,4,6-Trioxo-tetrahydro-pyrimidin-5-ylidene)-pentanal) undergoes cross-linking with chitosan resulting in the formation of BG-Chitosan. BG-Chitosan was found to be less soluble, hard and had greater swelling capacity compared to G-Chitosan.

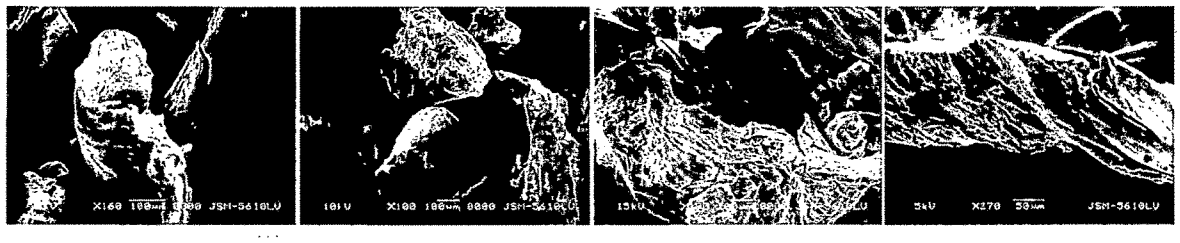

Figure 7.1. Scanning Electron Micrograph of C, BC, G-Chitosan and BG-Chitosan

Scanning Electron Micrograph of G-Chitosan displays an open porous and heterogeneous structure (Figure 7.1). Crosslinking with BG-Chitosan is seen to bring about conspicuous textural and morphological changes with BG-Chitosan forming a more compact and rigid structure. The pores are in the range 100 μm in G-Chitosan which reduce in BG-Chitosan to 50 μm.

7.2.2. Batch Adsorption Experiments.

A series of metal sorption experiments were conducted to study the effect of various parameters i.e. pH, dose and temperature for the removal of inorganic, methyl and phenyl mercury on C, BC, G-chitosan and BG-chitosan. For each experiment 25mL of Hg^{+2}, CH_3Hg^{+2} and $C_6H_5Hg^{+2}$ solution of known initial concentration and pH were taken in a 100mL stoppered conical flask. A suitable adsorbent dose was added to the solution and the mixture was shaken at

a constant speed. The supernatant was separated from the adsorbent by filtration and analyzed for the presence of unadsorbed Hg^{2+} by CVAAS (MA-5840 analyzer ECIL). All the experiments were conducted in triplicate and the average results are reported. The mercury uptake by chitosan was calculated as follows:

$$q_e = (C_i - C_e)/m; \quad (1)$$

where, C_i-initial concentration of metal ion mg/L; C_e – Equilibrium concn. of metal ion (mg/L); m – Mass of adsorbent (g/L); q_e – Amount of metal ion adsorbed per gram of adsorbent.

The experiments done without adsorbent were treated as blanks and they showed no precipitation of metal ions occurred under the conditions selected.

7.2.3. Selectivity Studies.

Selectivity coefficient of inorganic mercury over other inorganic cations like copper, cadmium and zinc were studied by batch procedure for C, BC, CL and BCL. The concentration of the metals was determined by ICP-AES (Thermo Jarrel Ash, Model TraceScan) at wavelengths of 409.014 nm. The selectivity of the mercury ions versus another cation was determined by shaking 100 mg of adsorbent with an aliquot of 10 mL each of 100 ppm of each individual inorganic ions (Cu^{2+}, Cd^{2+}, Zn^{2+} and Hg^{2+}) were taken at pH 4 to give a total volume of 40 mL. The selectivity coefficient ($S\,Hg^{2+}/M^{n+}$) is defined as

$$S_{Hg^{2+}/M^{n+}} = \frac{D_{Hg^{2+}}}{D_{M^{n+}}}$$

where DHg^{2+} and DM^{n+} are the distribution ratios of the mercury ion and other inorganic species, respectively. Distribution ratios were calculated using the formula

$$D_{M^{n+}} = \frac{C^{i}_{M^{n+}} - C^{f}_{M^{n+}}}{C^{f}_{M^{n+}}} \times \frac{v}{m}$$

where $C_i\,M^{n+}$ and $C_f\,M^{n+}$ are the concentrations of inorganic ions in aqueous phase before and after extraction, v is the volume of the solution, and m is the mass of the adsorbent. The percent extraction (%E) of inorganic ion is defined as

$$\%E = \frac{C^{i}_{M^{n+}} - C^{f}_{M^{n+}}}{C^{i}_{M^{n+}}} \times 100$$

7.3. Results and discussion

7.3.1. Uptake Studies.

7.3.1.1. ***pH dependence.*** Effect of pH was studied as a function of % uptake of the adsorbate under study (Hg^{+2}, CH_3Hg^{+2}, $C_6H_5Hg^{+2}$) in the range of pH 1-10, using metal ion concentration of 0.8mg/L with an adsorbent dose of 4g/L for C, BC, G-Chitosan and BG-Chitosan. There exists a large number of binding sites on C, BC, G-Chitosan and BG-Chitosan like amine, amide and hydroxyl groups. The nitrogen atom of the amino group and oxygen atoms of the hydroxyl groups can bind to a proton or a metal ion by electron pair sharing. The electronegativity of oxygen being more than that of nitrogen, the donation of lone pair of electrons from the nitrogen atom will be more facile than the oxygen atom for bond formation with mercury. In the case of chitosan under highly acidic condition (pH 1-2) there was no sorption of mercury because the binding sites are protonated which causes repulsion of the approaching mercury cation. As pH increases (3-7) the sorption of mercury increases because electron rich binding sites are exposed which allow the metal ions to get bound to the biosorbent [49].

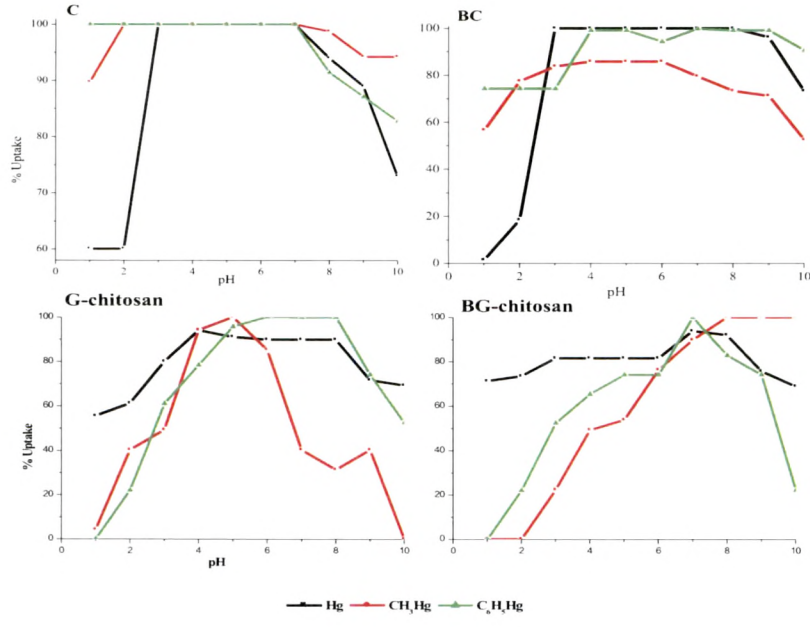

Initial metal conc. 0.1mg/L, amount of sorbent 4.0g/L, temperature 30^0C

Figure 7.2. Effect of pH on uptake of Hg^{2+}, CH_3Hg^{2+}, $C_6H_5Hg^{2+}$ using C, BC, G-Chitosan and BG-Chitosan

Inorganic Hg uptake was found to increase with increase in pH and reach equilibrium at pH 4 and 7 in case of G-Chitosan, BG-Chitosan respectively. Organic Hg uptake also was found to increase with increase in pH. Methyl mercury was found to reach equilibrium at pH 5, >8 in case of G-Chitosan, BG-Chitosan respectively while phenyl mercury was found to reach equilibrium at pH 6-8, 7 in case of G-Chitosan, BG-Chitosan respectively. This is in contrast to what is observed in general that adsorption of mercury decreases from pH 6 onwards due to precipitation [50]. This could be due to the fact that all the mercury species which are likely to exist in the investigated pH range (0.5–8), might remain in soluble form due to the low concentrations of mercury studied [51]. Furthermore, considerable uptake of Hg^{+2} is observed even under acidic pH conditions.

Beyond pH 7 sorption decreases due to precipitation as shown in Figure 7.2. At low and high pH, hydrogen bonding can also result between metal/mercuric hydroxide to hydroxyl groups of C, BC, G-chitosan and BG-chitosan. So the total uptake of mercury could be by electrostatic attraction, hydrogen bonding and weak van der Waals forces.

$$R - NH_2 + H^+ \leftrightarrow R - NH_3^+$$

$$R - NH_2 + Hg^{2+} \rightarrow R - NH_2Hg^{2+}$$

$$R - NH_3^+ + Hg^{2+} \rightarrow R - NH_2Hg^{2+} + H^+$$

In BC which has an amide group both C-N and C-O bonds possess comparable amounts of single and double bond character resulting in considerable delocalization of negative charge on the amide carbonyl oxygen atom causing predominant proton metal ion interactions. As the pH increases the hydroxyl groups become deprotonated resulting in negative charge

$$R - OH + OH^- \leftrightarrow R - O^- + H_2O$$

$$R' - O^- + Hg^{2+} \leftrightarrow R' - O - Hg^+$$

Thus due to stronger electrostatic attraction between the lone pairs of the nitrogen atom and Hg^{2+} and also the electrostatic attraction between the negatively charged hydroxyl group and positive or neutral mercury species, adsorption occurs in the pH range 3-7. The adsorption of Hg^{2+} at low pH values for C was found to be comparatively higher than BC, G-chitosan and BG-chitosan due to strong electrostatic attraction between the lone pair of nitrogen and Hg^{2+} species than the competing protons. The adsorption is higher in the case of BC with a concomitant increase in pH values due to deprotonation of amide groups and formation of covalent bonds between O, N and Hg.

7.3.1.2. ***Contact time dependence.*** The effect of agitation time on the uptake of Hg^{+2}, CH_3Hg^{+2}, and $PhHg^{+2}$ on G-Chitosan and BG-Chitosan is shown in Figure 7.3. Uptake study with respect to time showed >99% uptake after 3 h for C, whereas BC shows full uptake after 2 h, but the time needed to attain equilibrium is longer when using G-Chitosan than BG-Chitosan.

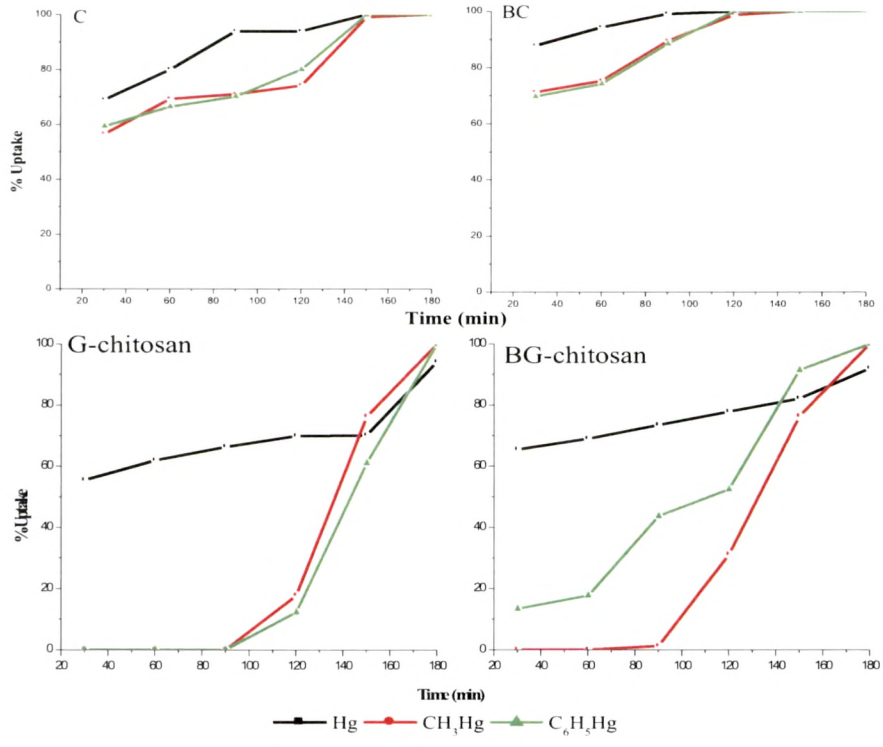

Initial metal conc. 0.1mg/L, amount of adsorbent 4.0 g/L, temperature 30^0C, optimum pH

Figure 7.3. Effect of Time on uptake of Hg^{+2}, CH_3Hg^{+2}, $C_6H_5Hg^{+2}$ using C, BC, G-Chitosan and BG-Chitosan

Hg^{2+} was found to adsorb at a faster rate with higher percentage removal than organic mercury ions. Since the mercury(II) ion has a smaller ionic radius, it is possible that mercury(II) ions diffuse faster through the adsorbent pores than the bulkier organic mercury. Also Hg^{+2} was found to adsorb at a faster rate followed by $C_6H_5Hg^{+2}$ and CH_3Hg^{+2}. More than 99% of total mercury was removed within a period of 120 min using BC, 160 min using C and 180 min using G-chitosan and BG-chitosan. This rapid initial binding rate suggests an instantaneous binding of

mercury on surface binding sites followed by slower and non specific binding to other components.

7.3.1.3. ***Temperature dependence.*** The effect of temperature on the sorption of Hg^{+2}, CH_3Hg^{+2}, $C_6H_5Hg^{+2}$ was studied by carrying out a series of experiments at 30-70^{0}C at equilibrium times of the respective sorbates. Figure 7.4 shows that effect of temperature on adsorption is different for both the adsorbates. Temperature studies (Figure 7.4) showed adsorption of inorganic mercury is endothermic in all the cases whereas adsorption of both the forms of organic mercury showed exothermic nature with all the adsorbents except C (endothermic).

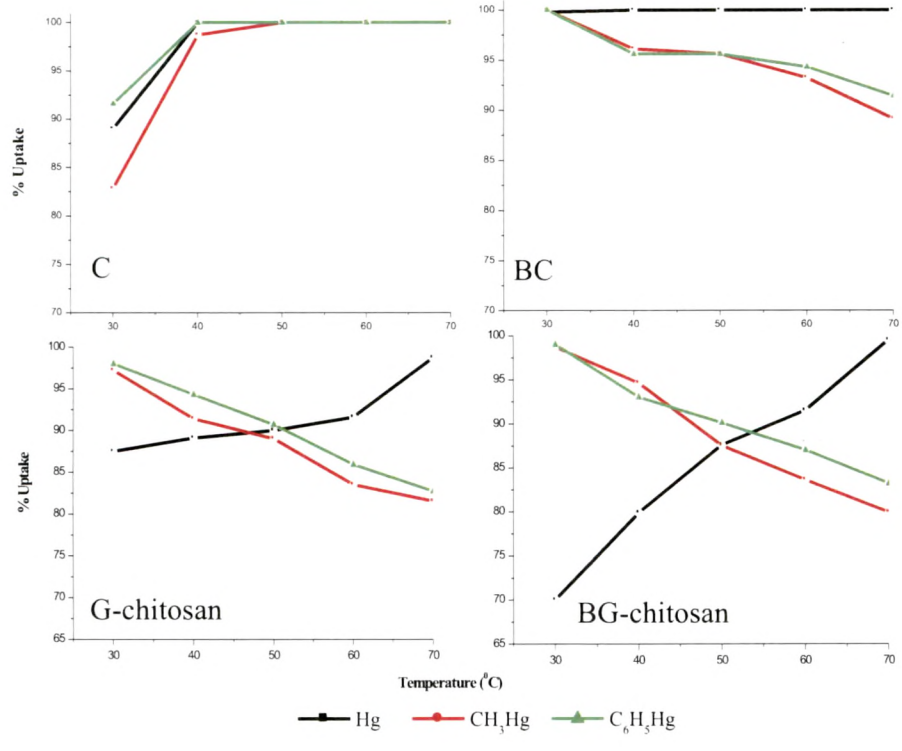

Initial metal conc. 0.1mg/L, amount of adsorbent 4.0 g/L, optimum pH, 180 min

Figure 7.4. Effect of Temperature on uptake of Hg^{+2}, CH_3Hg^{+2}, $C_6H_5Hg^{+2}$ using C, BC, G-Chitosan and BG-Chitosan

Uptake of inorganic mercury was found to increase with increase in temperature in the case of all the sorbents under study C, BC, G-Chitosan and BG-Chitosan but sorption of organic mercury decreased with increase in temperature for BC, G-Chitosan and BG-Chitosan suggesting chemisorption mechanism in the latter case [52]. Whereas increase in inorganic mercury adsorption with increasing temperature might be due to an enhanced rate of intraparticle diffusion of the adsorbate, as diffusion is an endothermic process. Chemisorption in case of organomercury can be explained due to the greater softness of organomercury compounds.

7.3.2. Adsorption Isotherms.

The adsorptive capacity of chitosan derivatives used for mercury removal was determined through adsorption isotherm studies. The Langmuir and Freundlich models were used to determine the adsorption capacity of mercury on chitosan derivatives and model parameters are presented (Table 7.2 and Figure 7.5).

From the correlation coefficient values (r^2) obtained for the two models, it can be seen that the Langmuir and Freundlich models cannot be applied to these data. Both Langmuir and Freundlich models could not be applied to the data obtained for mercury using chitosan based adsorbents. This could be due to mercury ions penetrating the adsorbent, adsorbing onto amine/ amide sites and forming metal clusters which might block the pores. This might render the active sites lying in the interior inaccessible for adsorption.A similar behavior was observed by Gregory et al. during the study of Cd^{2+} ions on porous magnetic chitosan beads [53]. The negative values obtained for Gibbs free energy, enthalpy and entropy suggest that the adsorption process is feasible and spontaneous in the case of G-Chitosan and BG-Chitosan.

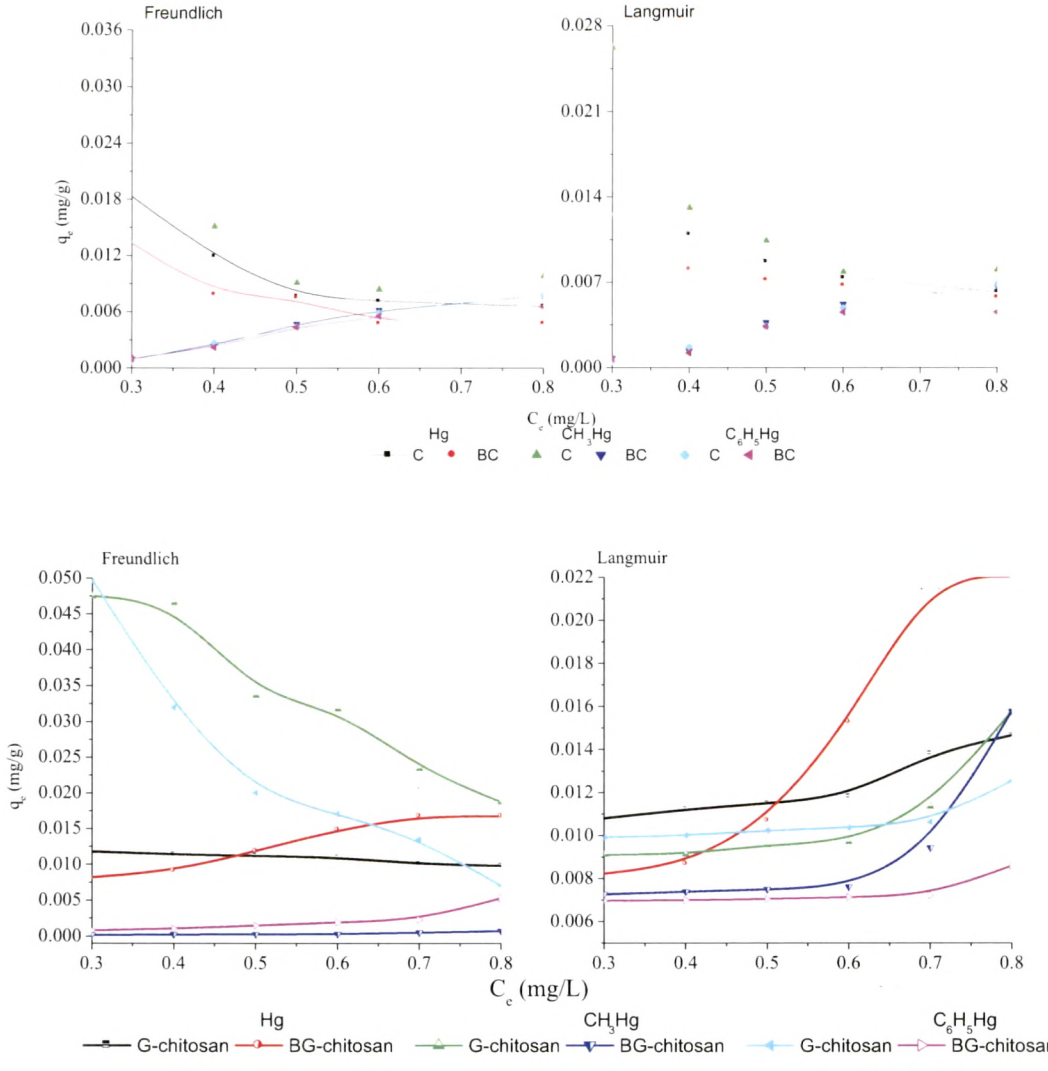

Figure 7.5. Freundlich and Langmuir Isotherm plots for C and BC

7.3.3. Adsorption Kinetics.

In order to investigate the possible mechanism of sorption process three kinetic models were used including Pseudo first order model, Pseudo second order model and Intra-particle diffusion model. Kinetics was examined for the sorption of Hg^{2+}, CH_3Hg^{2+}, and $PhHg^{2+}$ on chitosan derivatives under study using a series of measurements extending from 30 min to 240 min at 25 ^{0}C (Table 7.2 and Figure 7.6).

Table 7.2. Isothermal and kinetic parameters for adsorption of inorganic and organic mercury

Kinetics and Isotherms		C			BC		
		Hg^{2+}	CH_3Hg^+	$C_6H_5Hg^+$	Hg^{2+}	CH_3Hg^{2+}	$C_6H_5Hg^+$
Pseudo 1st order	q_e (mg/g)	0.0410	0.0330	0.0650	1.1980	0.0100	1.0140
	K (min^{-1})	0.2000	0.1000	0.2300	0.1500	0.0790	0.0010
	r^2	0.9590	0.9700	0.9520	0.9850	0.8170	0.9190
Pseudo 2nd order	q_e (mg/g)	0.0500	0.0620	0.0540	0.0294	0.0023	0.00129
	K (g/mgmin)	0.2480	0.0670	0.2810	0.5090	107.70	4.1500
	r^2	0.9680	0.8960	0.9900	0.9950	0.6040	0.7130
Intra-particle	K_i($mg/gmin^{0.5}$)	0.0030	0.0030	0.0440	0.0020	0.0008	0.0011
	r^2	0.9810	0.9790	0.9080	0.9860	0.9800	0.9990
Langmuir	q_m (mg/g)	0.0130	0.0100	0.0250	0.0040	0.0060	0.0200
	K_a (L/mg)	-184.0	-156.0	-927.0	-887.3	-73.5	-179.3
	r^2	0.9300	0.9450	0.9850	0.9940	0.9440	0.9560
Freundlich	K_f $(mg/g)(dm^3/mg)^{1/n}$	0.455	0.0002	0.004	0.003	$4.4x10^{-5}$	$5.4x10^{-5}$
	N	-1.790	-0.9360	-8.880	-3.3400	-0.1790	-0.9860
	r^2	0.8700	0.8670	0.9960	0.8010	0.7050	0.9130

Kinetics and Isotherms		G-Chitosan			BG-Chitosan		
		Hg^{+2}	CH_3Hg^{+2}	$C_6H_5Hg^{+2}$	Hg^{+2}	CH_3Hg^{+2}	$C_6H_5Hg^{+2}$
Pseudo 1st order	q_e (mg/g)	0.0170	0.0151	0.0190	0.0355	0.0295	0.0478
	K (min^{-1})	0.0090	0.0081	0.0102	0.0195	0.0018	0.0213
	r^2	0.9170	0.9560	0.9290	0.9490	0.9590	0.9880
Pseudo 2nd order	q_e (mg/g)	0.0210	0.2310	0.2030	0.0625	0.0591	0.0716
	K (g/mgmin)	0.5600	0.6730	0.4950	0.0001	0.0003	0.0002
	r^2	0.9170	0.9210	0.9330	0.9100	0.9230	0.9190

Intra-particle	K_i(mg/gmin$^{0.5}$)	0.001	0.0008	0.0021	0.0018	0.0076	0.0082
	r^2	0.9780	0.9890	0.9880	0.9920	0.9230	0.8190
Langmuir	q_m (mg/g)	0.0080	0.0089	0.0098	0.0065	0.0072	0.0069
	K_a (L/mg)	228.10	234.50	257.80	240.50	189.57	314.00
	r^2	0.9940	0.9800	0.9960	0.9680	0.6670	0.8190
	ΔG (KJ/mol)	-13.70	-13.75	-13.99	-13.81	-13.21	-14.48
Freundlich	K_f (mg/g)(dm^3/mg)$^{1/n}$	0.0530	0.0817	0.0919	0.0008	0.0001	0.0006
	N	2.7800	3.1400	1.5670	1.815	2.321	1.513
	r^2	0.4760	0.5140	0.6780	0.9490	0.9590	0.8990

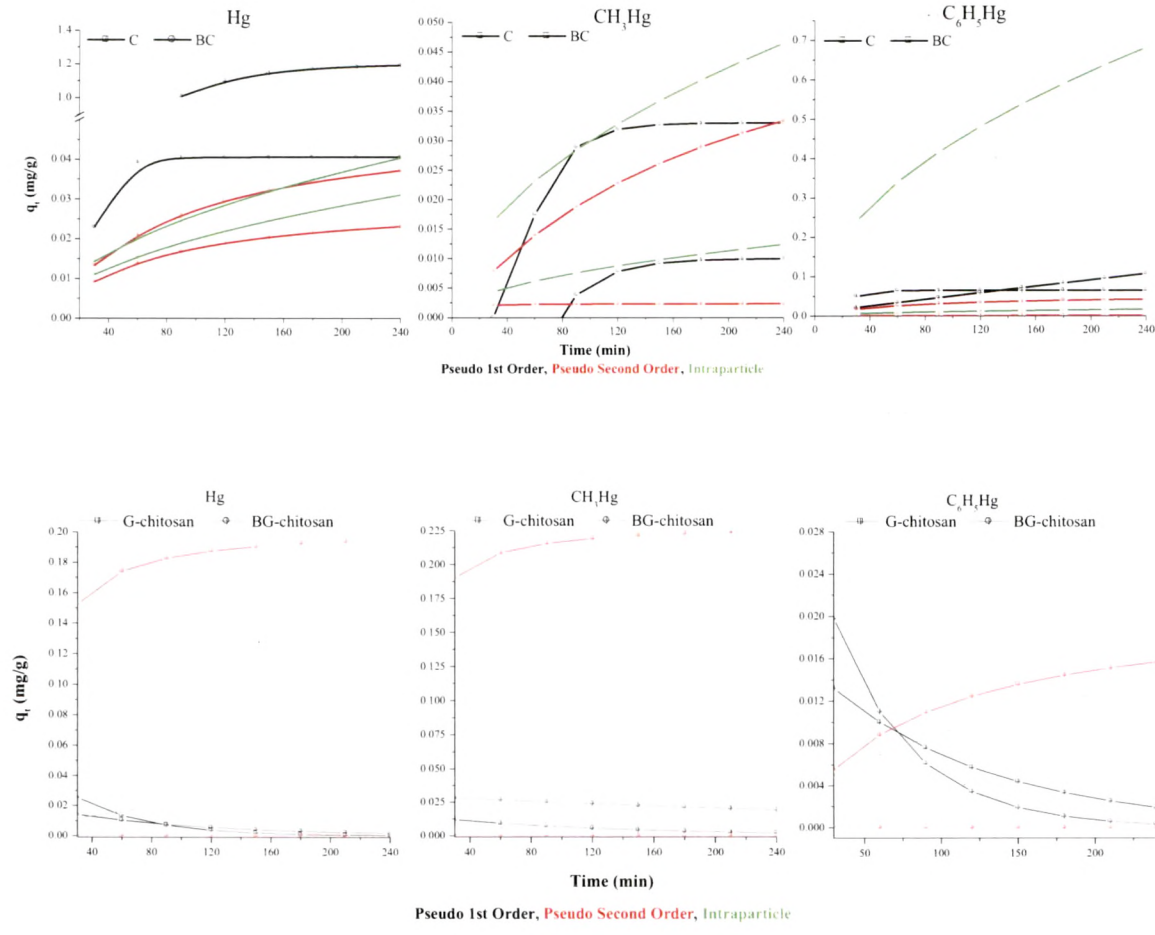

Figure 7.6. Different Kinetic plots for C, BC, G-chitosan and BG-chitosan

Pseudo first order model was fitted with a correlation coefficient of >0.917 for all the three forms of mercury. Values of regression coefficients are shown in Table 7.2. It is seen that the rate of adsorption is fast for the adsorbents under study in the case of Hg^{2+}, CH_3Hg^{2+}, and $C_6H_5Hg^{2+}$ adsorption. However the time needed to attain equilibrium is longer when using C, G-chitosan and BG-chitosan than BC (120 min using BC, 160 min using C and 180 min using G-chitosan and BG-chitosan). This could be explained by the presence of a larger number of functional groups for bonding in the case of BC (potentiometric titrations and FTIR). However Hg^{2+} was found to adsorb at a faster rate followed by CH_3Hg^{2+} and $C_6H_5Hg^{2+}$. This could be due to the smaller ionic radius of Hg^{2+} which enables it to diffuse faster than the bulkier $C_6H_5Hg^{2+}$ and CH_3Hg^{2+}. More than 99 % of total mercury was removed within the period of 180 min. This rapid initial binding rate suggests an instantaneous binding of mercury on surface sites followed by slower and non specific binding to other components.

But in the case of Pseudo 2^{nd} order rate equation the correlation coefficients were found to be >0.90. Intraparticle diffusion mechanism was found to be followed by G-Chitosan for all the three species of mercury but in BG-Chitosan phenyl mercury did not follow intraparticle diffusion whereas others did with a correlation coefficient >0.92. This suggests that multiple mechanisms like fast ion exchange, inter and intra-molecular binding and diffusion are operating in the sorption of mercury on C, BC, G-Chitosan and BG-Chitosan.

7.3.4. FTIR Spectroscopy.

Typical absorption frequencies of FTIR for C, BC, G-Chitosan, BG-Chitosan and mercury loaded species with their corresponding assignments are summarized in Table 7.3.

The strong broad band in region of 3300 to 3500 cm^{-1} is characteristic of the N-H stretching vibration in C, BC, G-Chitosan and BG-Chitosan although there is the possibility of overlapping between the N-H and the O-H stretching vibrations corresponding to pyranose structure. For BC the FTIR spectra shows a peak at 1654 cm^{-1} specifically for the amide groups indicating the grafting of barbital on chitosan. The band corresponding to free amino groups is observed at 1632, 1629.95 and 1599.31cm^{-1} for C, G-Chitosan and BG-Chitosan respectively.

Table 7.3. Typical absorption frequencies of infrared spectra of the C and BC

Sample	C/ BC	C/BC-Hg	C/BC-CH_3Hg	C/BC-PhHg	Assignment
Wave numbers (cm^{-1})	3447/ 3425	3432/ 3449	3445/ 3432	3441/ 3435	N-H & OH Stretching
	2929/ 2924	2920/ 2924	2921/ 2924	2921/ 2923	C-H stretching
	1632/1654	1599/ 1636	1597/ 1636	1597/ 1637	N-H bending
	-/ 1560	-/ 1512	-/ 1511	-/ 1509	N-H bending
	1383/ 1380	1384/ 1384	1383/ 1384	1383/ 1382	C-H bending
	1074/ 1073	1086/ 1077	1089/ 1024	1090/ 1080	C-N, C-O stretch
Samples	G-chitosan	G-chitosan-Hg	G-chitosan-CH_3Hg	G-chitosan-PhHg	Assignment
Wave numbers (cm-1)	3434/ 3431	3431/ 3431	3431/ 3427	3431/ 3433	N-H Stretching
	2925/ 2924	2933/ 2933	2924/ 2926	2926/ 2926	C-H stretching
	1725/ -	1685/ -	1651/ -	1757/ -	C=Ostretching(Aldehyde)
	1629/ 1599	1635/ 1635	1599/ 1618	1637/ 1637	N-H bending
	1379/ 1380	1384/ 1384	1384/ 1383	1383/ 1383	C-H bending
	-/ 1153	-/ 1155	-/ 1159	-/ 1155	C-N, C-O Stretching
	1074/ 1084	1066/ 1070	1068/ 1029	1062/ 1063	C-N, C-O Stretching

But the frequency is shifted to a lower wave number in case of BG-Chitosan due to consumption of these groups during cross linking of chitosan with 5-(2,4,6-Trioxo-tetrahydro-pyrimidin-5-ylidene)-pentanal, the condensation product of glutaraldehyde and barbital. A band at 1725cm^{-1} in G-Chitosan can be attributed to carbonyl groups of unreacted aldehyde functional groups of glutaraldehyde which are found to be absent in BG-Chitosan suggesting the condensation of these aldehydic groups of gltaraldehyde with barbiturate. A new band in BG-Chitosan at 1153cm^{-1} appeared due to the formation of new C-N bonds after complexation of glutaraldehyde with barbital and cross-linking with chitosan. This 1153cm^{-1} peak can be attributed to asymmetric stretching of C-O-C and C-N stretch.

The amide stretching frequency shifts from 1654 cm^{-1} to a lower frequency of 1636 cm^{-1} after mercury adsorption showing the possible interaction of metal linkage with O and N of the amide group [54]. The FTIR spectra after sorption of mercury on G-Chitosan shows a shift in 1725cm^{-1} band to 1655 and 1700cm^{-1} after mercury binding in case of Hg^{+2} and $CH3Hg^{+2}$ respectively suggesting the involvement of carbonyl arising from unbound sites of

glutaraldehyde in binding of mercury. This behavior is consistent with previous reported results on uranium removal by chitosan and molybdate removal by cross-linked chitosan beads [55]. A decrease in transmittance in the wave number region of 3434 to 3431cm^{-1} after mercury sorption indicates that N-H vibration was affected due to sorption of mercury. In the case of BG-Chitosan the FTIR data showed that C-N stretching frequency at wave number of 1084cm^{-1} shifted to 1070, 1028, 1062cm^{-1} after mercury sorption suggesting the attachment of mercury to N and O bond of amide moiety A shift in the band at 1153cm^{-1} to higher wavenumbers was also observed in BG-Chitosan suggesting that N and O of amide involved in the sorption process. After mercury sorption there is a large shift in N-H bending absorption frequency from 1599cm^{-1} to 1635cm^{-1}, 1618cm^{-1} and 1637cm^{-1} for Hg^{+2}, CH_3Hg^{+2} and $PhHg^{+2}$ respectively in BG-Chitosan. A shift in 1074cm^{-1} band to 1066cm^{-1}, 1068cm^{-1} and 1062cm^{-1} related to C-N stretching indicates that nitrogen atoms are main sorption sites in both. Thus all the bands are suggestive of involvement of bonds with N atoms and C=O of unreacted aldehyde in the case of G-Chitosan and C-N and C-O of amide in BG-Chitosan for sorption mercury.

Thus we can conclude that for G-Chitosan sorption sites may be free aldehyde group of glutaraldehyde which has not been used in cross linking of chitosan and amino groups in chitosan. In the case of BG-Chitosan the sorption sites could be amide groups of barbital where mercury can coordinate bidentately to both amide nitrogen and oxygen atoms [56].

Frequencies for N-H stretching and bending were found to decrease after mercury adsorption in the case of C and BC showing the bonding of Hg^{2+} with the N of amine where the lone pair of electrons of the nitrogen atom was donated to the shared bond between the N and Hg^{2+} and as a consequence, the electron cloud density of the nitrogen atom was reduced, causing the shift. Mercury adsorption is found to affect the frequencies of all the bonds with N atoms of amine and amide, indicating that nitrogen atoms (amine group) are the main adsorption sites for mercury adsorption on C while in the case of BC it is N and O (amide and amine group).

7.3.5. Data analysis.

Results of potentiometric titration curves are used to generate a simplified mathematical model using Matlab [57-59].

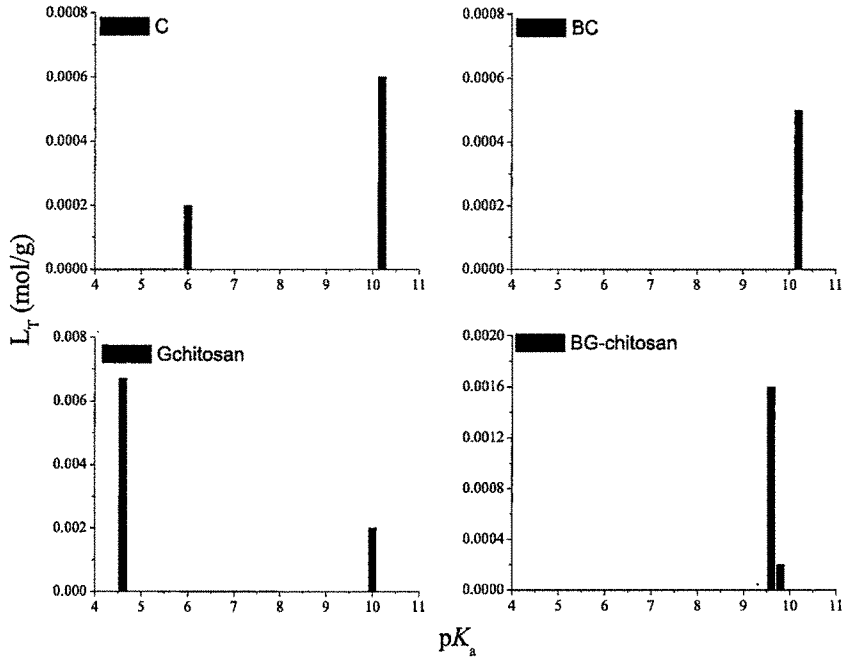

Figure 7.7. pK_a spectra determined by linear programming analysis

The pK_a spectra resulting from fitting the data using weighted mean value calculations are shown in Figure 7.7 and Table 7.4.

Table 7.4. Three-Site model from pK_a Analysis of C & BC Titration Data by Linear Programming

Ligand Class		1	2
Range of pK_a		4.0– 7.0	9.7 – 11.0
Functional Group		Self assembled amine/ protonated amine	Hydroxyl/ Amine
Chitosan	pK_a	10.2	-
	L_T	0.0006 mol/g	-
BC	pK_a	-	10.2
	L_T	-	0.0005 mol/g
G-chitosan	pK_a	4.6	10.0
	L_T	0.0067	0.0020 mol/g
BG-chitosan	pK_a	-	9.7
	L_T	-	0.0009 mol/g

Surface pK_a values for Site 1 falls in the range of 4-7 pK_a which have been reported for amino groups in self-assembled monolayers or protonated amines. Usually high pK_a sites (~10) are attributed to phenolic hydroxyl sites. Since both C and BC do not have phenolic protons, it is likely that high pK_a sites are for CH_2OH groups, or for 1^0 or 2^0 amines which have pK_a values in the range 9-11. In summary the pK_a sites that are observed here are likely to correspond to site 1 amino groups in self assembled monolayers or protonated amines, for site 2 it corresponds to hydroxyl or amines.

7.3.6. Specificity studies.

The % extraction, distribution ratio and selectivity coefficients of mercury ion with respect to metal ions like Cu^{2+}, Cd^{2+} and Zn^{2+} using C, BC, CL and BCL are studied.

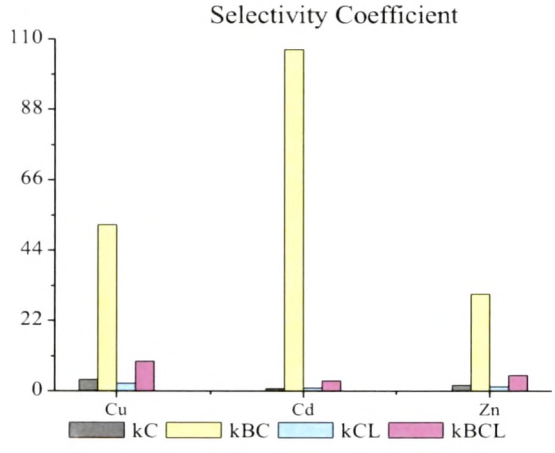

Figure 7.8. % Extraction, Distribution Coefficient and Selectivity coefficient

The obtained results are depicted in Figure 7.8. It is clear from the results that BC shows good selectivity for mercury (102) as compared to C, CL and BCL in the concentration range studied. A significant difference between the binding of mercury ion and other competitor metal ions on the adsorbents under study can be explained on the basis of Pearson's classification [60] according to which mercury is the softest of the metals which have been studied and can attach to soft bases (functional groups) present in the materials under study.

7.4. Conclusions

New adsorbents C, BC, G-chitosan and BG-Chitosan were prepared. BG-Chitosan was found more rigid and had more swelling capacity compared to other sorbents under study. Grafting barbital on C improves the equilibrium time for uptake of phenyl, methyl and inorganic Hg^{2+} when compared. Mercury adsorption to C, BC, G-chitosan and BG-Chitosan are strongly pH-dependent. There must be more than one mechanism responsible for mercury removal. Sorption of all the three forms of mercury showed similar behavior except for the fact that the process is endothermic for Hg^{+2} and exothermic for CH_3Hg^{+2}, $C_6H_5Hg^{+2}$. C showed higher adsorption capacity as compared to other sorbents under study. Amine, amide, amine and aldehyde, amide groups are involved in binding through complexation, weak van der Waals forces and electrostatic interactions in C, BC, G-Chitosan and BG-Chitosan respectively. More than 99 % of total mercury was removed within 160 min suggesting instantaneous binding of mercury on surface sites followed by slower and non specific binding to other components. Due to the different nature of the adsorbate-adsorbent system and the low initial metal ion concentration used comparison with other adsorbents is not possible. Appreciable selectivity was obtained for mercury with BC as adsorbent.

Literature Cited.

1. A. Demirbas. *Energy Edu. Sci. Technol.* **2000**, *5*, 21.
2. A. Demirbas. *Energy Edu. Sci. Technol.* **2000**, *6*, 19.
3. U.K. Garg, M.P. Kaur, V.K. Garg, D. Sud. *Biores. Technol.* ***in press.***
4. U.K. Garg, M.P. Kaur, V.K. Garg, D. Sud. *J. Hazard. Mater.* **2007**, *140*, 60.
5. E. Sjotrom. Wood Chemistry Fundamentals and Applications. *Academic Press Inc., New York* **1981.**
6. T.J. Beveridge, R.G.E. Murray. *J. Biotechnol.* **1980**, *141*, 876.
7. V.K. Gupta, I. Ali. *J. Colloid Interface Sci.* **2004**, *271*, 321.
8. Y. A. Koyama, C. P. Taniguchi, B. D. W. Haung. *Journal of Applied Polymer Science,* **1986**, *31*, 1951.
9. K. Kurita, T. Sannan, Y. J. Iwakura. *Applied Polymer Science* **1979**, *23*, 511.
10. J. D. Merrifield, W. G. Davids, J. D. MacRae, A. Amirbahman. *Water Research* **2004**, *38*, 3132.
11. A. Zhang, J. Xiang, L. Sun, S. Hu, P. Li, J. Shi. *Industrial Engineering & Chemistry Research* **2009**, *48*, 4980.
12. R. S. Vieira, M. M. Beppu. *Adsorption.* **2005**, *11*, 731.
13. K. Oshita, M. Oshima, Y. H. Gao, K. H. Lee, S. Motomizu. *Analytical Sciences* **2002**, *18*, 1121.
14. J. Choong. *Journal of Microbiology and Biotechnology* **2005**, *15*, 497.
15. J. Choong, W.H. Holl. *Water Research,* **2003**, *37*, 4770.
16. E. Guibal. *Industrial Engineering & Chemistry Research,* **1998**, *37*, 1454.
17. R. A. A. Muzzarelli, O. Tubertini. *Talanta* **1969**, *16*, 1571.
18. P. Miretzky, A. Fernandez Cirelli. *Journal of Hazardous Materials* **2009**, *167*, 10.
19. A.J. Varmaa, S.V. Deshpandea, J.F. Kennedy. *Carbohydrate Polymers* **2004**, *55*, 77.
20. A. Bhatnagar, M. Sillanpaa. *Advances in Colloid and Interface Science* **2009**, *152*, 26.
21. R.S. Vieira, M.M. Beppu. *Colloids and Surfaces A: Physicochem. Eng. Aspects* **2006**, *279*, 196.
22. L.M. Zhou, Y.P. Wang, Q.W. Huang. *J. Nucl. Radiochem.* **2007**, *29*, 184.
23. L. Zhou, Y. Wang, Z. Liu, Q. Huang. *J. Hazard. Mater.* **2009**, *161,* 995.

24. G. Cardenas, P. Orlando, T. Edelio. *International Journal of Biological Macromolecules* **2001**, *28(2)*, 167.
25. R. Qu, C. Sun, F. Ma, Y. Zhang, C. Ji, Q. Xu, C. Wang, H. Chen. J. Hazard. Mater. 167 (2009) 717–727.
26. K. Campos Gavilan, A.V. Pestov, H. Maldonado Garcia, Y. Yatluk, Jean Roussya, E. Guibal. *Journal of Hazardous Materials* **2009**, *165*, 415.
27. A.M. Donia, A.A. Atia, K.Z. Elwakeel. *J. Hazard. Mater.* **2008**, *151*, 372.
28. J.D. Merrifield, W.G. Davids, J.D. MacRae, A. Amirbahman, *Water Res.* **2004**, *38*, 3132.
29. C. Jeon, W.H. Holl, *Water Res.* **2003**, *37*, 4770.
30. A. Khan, S. Badshah, C. Airoldi. *Colloids and Surfaces B: Biointerfaces* **2011**, *87*, 88.
31. K.D. Trimukhe, A.J. Varma. *Carbohydr. Polym.* **2008**, *71*, 66.
32. J.L. Barriada, R. Herrero, D.P. Rodriguez, M.E. Sastre de Vicente. *Reactive & Functional Polymers* **2008**, *68*, 1609.
33. L. Wang, R. Xing, S. Liu, S. Cai, H. Yu, J. Feng, R. Li, P. Li. *International Journal of Biological Macromolecules* **2010**, *46*, 524.
34. R.A.A. Muzzarelli, R. Rocchetti. *J. Chromatogr. A* **1974**, *96*, 115.
35. J.D. Merrifield, W.G. Davids, J.D. MacRae, A. Amirbahman. *Water Res.* **2004**, *38*, 3132.
36. A. Zhang, J. Xiang, L. Sun, S. Hu, P. Li, J. Shi, P. Fu, S. Su. *Ind. Eng. Chem. Res.* **2009**, *48*, 4980.
37. R.S. Vieira, M.M. Beppu. *Adsorption* **2005**, *11*, 731.
38. K. Oshita, M. Oshima, Y.H. Gao, K.H. Lee, S. Motomizu. *Anal. Sci.* **2002**, *18*, 1121.
39. J. Choong. *J. Microbiol. Biotechnol.* **2005**, *15*, 497.
40. J. Choong, W. H. Holl. *Water Res.* **2003**, *37*, 4770.
41. W. M. Arguelles, C. C. Peniche. *Appl. Macromol. Chem. Phys./Angew. Makromol. Chem.* **1993**, *207*, 1.
42. C. C. Peniche, L. W. Alvarez, W. M. Arguelles. *J. Appl. Polym. Sci.* **2003**, *46*, 1147.
43. R. A. A. Muzzarelli, I. Antonio. *Water, Air Soil Pollut.* **1971**, *1*, 65.
44. C. Karol, E. Guibal, P. Francisco, M. Ly, M. Holger. *Adv. Mater. Res.* **2007**, *20-21*, 635.
45. G. M. Gadd. Biosorption. *Chem. Ind.* **1990**, *13*, 421.
46. L. Nan, B. Renbi, L. Changkun. *Langmuir* **2005**, *21*, 11780.

47. P. Padmaja. Concentration, separation and determination of trace amounts of Hg. Ph.D. Thesis, IIT Madras, 1994.
48. P. Ahuja, R. Gupta, B. K. Saxena. Zn^{+2} biosorption by Oscillatoria anguistissima. *Process Biochem.* **1999**, *34*, 77.
49. M. D. Ahmed, A. A. Asem, M. Heniesh. *Separation and Purification Technology* **2008**, *60*, 46.
50. C. F. Baes Jr., & R. E. Mesmer. The hydrolysis of cations. New York: *Wiley* **1976**, 301.
51. F. Jonathan, N. K. Aline, S. Jaka, J. Yi-Hsu, I. Nani, I. Suryadi. *Journal of Hazardous Materials* **2009**, *162*, 616.
52. L. R. Gregory, H. Tzu-Yang. *Ind. Eng. Chem. Res.* **1993**, *32*, 2170.
53. S. Hasan, A. Krishnaiah, T. K. Ghosh, D. S. Viswanath. *Ind. Eng. Chem. Res.* **2006**, *45*, 5066.
54. R. A. A. Muzzarelli. *Carbohydrate Polymers* **2011**, *84*, 54.
55. T. Hui-Chung, L. Carmay. *Journal of Physical Chemistry A* **2006**, *110*, 452.
56. P. Brassard, J. R. Kramer, P. V. Collins. *Environ. Sci. Technol.* **1990**, *24*, 195.
57. J. S. Cox, D. S. Smith, L. A. Warren, F. G. Ferris. *Environ. Sci. Technol.* **1999**, *33*, 4514.
58. M. Dittrich, S. Sibler. *Langmuir* **2006**, *22*, 5435.
59. I. Sokolov, D. S. Smith, G. S. Henderson, Y. A. Gorby, F. G. Ferris. *Environ. Sci. Technol.* **2001**, *35*, 341.
60. R.G. Pearson. *J. Am. Chem. Soc.* **1963**, *85*, *3533*.

Chapter 8

Preparation and characterization of Specific Adsorbent for Uranium

Outline:

8.1. Introduction

Molecular imprinting polymers (MIP) which have the ability for high selective adsorption of target chemical species from various media are presently of great interest [1, 2]. In recent years, some imprinting polymers have been prepared and used for selective removal, pre-concentration and extraction of metal ions [3-20] which are termed as ion imprinting polymers (IIP).

The high selectivity of these imprinted polymers arises from the memory effect of the polymer to the imprinted ions, including the specificity of interaction of ligand with the metal ions, the coordination geometry and coordination number of metal ions, the charge of the metal ions, and the size of the metal ions [21].

Important steps for synthesis of imprinted polymer include selection of a functional monomer that can form a complex with template, polymerization of the monomer containing imprint ion and leaching of the imprint ion to obtain an imprint which can recognize the template from a mixture of chemical species (Scheme 8.1). The bonding between the template and the functional monomer can be either covalent or non-covalent.

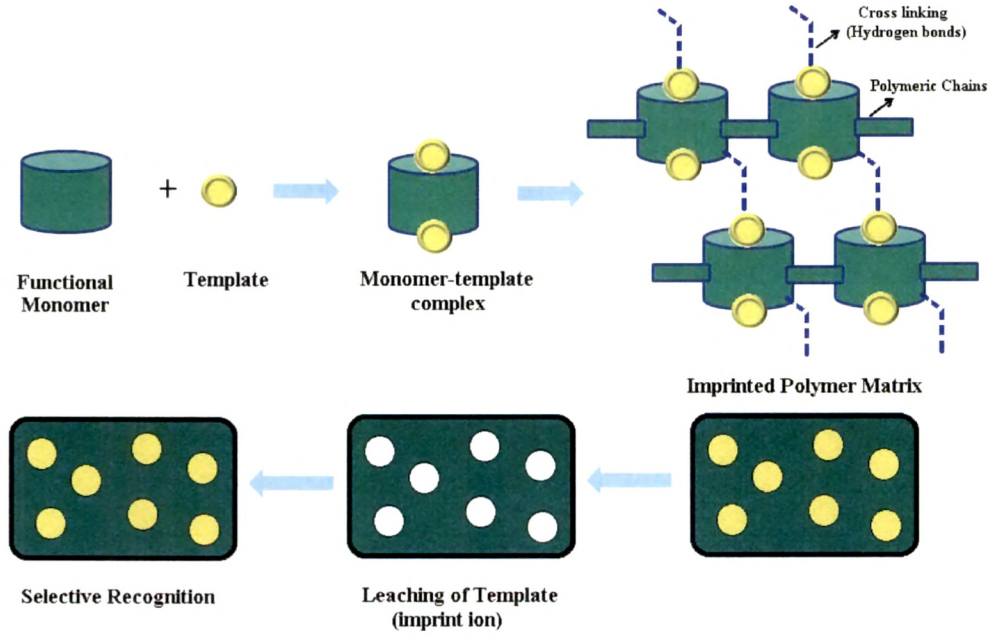

Scheme 8.1. Scheme for complexation involving template, imprinting by formation of matrix, leaching of template and selective recognition

Hydrogen bonding is the most common interaction during non-covalent molecular imprinting. Previous studies have shown that an imprinted polymer prepared based on hydrogen bonding interactions lost its molecular recognition ability in aqueous media or organic solvents with high polarity [21, 22]. The covalent bonding system employs a template-monomer complex which is formed by a reversible covalent bonding.

Traditionally, MIPs, prepared by bulk polymerization, exhibit highly selective recognition but with poor site accessibility to the target molecules, as the template molecules and functional groups are totally embedded inside the polymer network and the binding kinetics is low [23]. They also have other limitations such as non-uniform distribution of particle size [24, 25-27], high consumption of template and material [25, 27, 28] thermal instability, and swelling and shrinkage effects [26]. Therefore, much attention has been paid to novel surface imprinting techniques which offer fast mass transfer kinetics [29-36]. Recently, the problems associated with bulk polymerization have also been overcome by grafting techniques wherein the MIPs layers are coated onto substrates with known surface morphologies [27, 28, 38-41]. We were interested in the development and evaluation of the grafting of ion imprinting oligomers onto agrowaste materials.

Industrial activities and mining operations have exposed man to the toxic effects of uranium. Uranium is an emerging pollutant and can cause irreversible renal injury and may lead even to death. Due to the biological, environmental and industrial impacts of uranyl ion, development of imprinting polymers for selective separation of uranyl ion is of continuing interest [3-20].

In the race of nuclear empowerment, every country is consuming more and more of nuclear fuel leads to increased incidents of seepage and residual fuel and distribution of radioactivity to the our surroundings. Recently number of reports has focused on uranium poisoning. Times Of India (TOI) reported in March 2009 high levels of uranium while analyzing the hair and urine samples of ~150 children in Punjab. Children were reported to be affected from birth with physical deformities, neurological and mental disorders. Further, TOI of June 2010 reported that studies carried out amongst mentally retarded children of Punjab, revealed uranium levels high enough to cause diseases. The recent Fukushima Nuclear accident in March 2011, resulted in a hovering radioactive cloud and seepage of fuel to the sea water. Hence

selective extraction and recovery of uranium from these discharges is essentially required in view of its extreme toxicity and environmental aggressiveness.

The combination of cross-linking with macromolecular functional monomers for production of selective imprinted polymers for uranium ion which does not exhibit directional bonding, prepared by bulk polymerization, ATRP, Free radical copolymerization, cross linked matrix, thermal polymerization and sol-gel surface imprinting etc. are summarized in Table 8.1.

Table 8.1. Summary of Retention capacity/ Distribution Coefficient for uranium

Sr. No.	Functional monomer/ Polymer	Technique	Cross Linker	pH	Eluent	Retention capacity/ Distribution Coefficient		References
						Imprinted sorbent	Control Sorbent	
1.	MAA	Free Radical	EGDMA	3.0	1M HCl	4950.0	35.5	[3]
	HEMA/ VP/ Amidoxime	Free Radical	EGDMA	8.0	1N HCl	26 µmol/g	-	
2.	Chitosan	-	Glutraldehyde/ glyoxal	4.0	1:1 HCl	-	-	[42]
3.	2-chloroacrylic acid	Free Radical	EGDMA	<3.0	Conc. HNO_3	-	-	[5]
4.	TMOS	Sol-Gel (Surface imprinting)	-	~5.0	HNO_3	-	-	[6]
5.	DCQ/ Styrene	Thermal	DVB	6.0	1:1HCl	99.0	3.16	[8]
6.	Quinoline-8-ol/ DCQ/ DBQ/ DIQ/ VP/ Styrene	Free Radical	DVB	6.0	1:1HCl	30 mg/g	-	[9]
7.	DCQ/ VP/ Styrene	Free Radical	DVB	6.0	1MHCl	34 mg/g	25 mg/g	[10]
8.	VP/ Styrene	Free Radical	DVB	6.0	1MHCl	886.3	-	[12]
9.	SALO/ Catechol/ succinic acid/ DCQ/ VP/ HEMA	Free Radical	EGDMA	>5.0	5MHCl	99x5x10E+4	-	[13]
10.	SALO/ VP/	Free	DVB	~3.	1MHCl	99x5x10E	0.15x5x10E	[14]

	Styrene	Radical		5		+3	+3	
11.	Chitosan/ PVA	Cross Linking	EG diglycidyl ether	5.0	0.1MHNO3	495.0	86.0	[15]
12.	SALO/ VP/ DCQ	Thermal	DVB	7.0	5.0MHCl	-	-	[16]
13.	PPMP/ MAA	Thermal	EGDMA	3.0	5MHCl	37.58 mg/g	25.44 mg/g	[43]
14.	VBA/ Styrene	Free Radical	DVB	3.0	$1MHNO_3$	-	-	[44]
15.	Piroxicam/ VP/ Styrene	Free Radical	DVB/ EGDMA	6.0	6MHCl:MeOH (1:1)	38.58 mg/g, 14.0	-	[17]
16.	SALO/ VP/ 2-methoxy ethanol/ Methacrylic acid	Thermal	EGDMA	5.0	2MHCl	-	-	[18]
17.	3-(Triethoxysilyl) propylacrylamide/ acrylamide (Aam)/ (TEA)/ 3-(triethoxysilyl)propyl acrylate/ PVC	Sol-Gel	TEOS	-	$12\%HNO_3$ in ultra-sonicator	-	-	[45]
18.	VP/ HEMA	Thermal/ Surface imprinting	EGDMA	5.0 - 7.0	1MHCl	97.1 µmol/g	-	[19]
19.	1-hydroxy-2-(prop-20-enyl)-9,10-anthraquinone	Free Radical	EGDMA	1.0 - 3.0	2MHCl	52.1 µmol/g	-	[20]

However, most of these IIPs are not suitable for removal of uranium from nuclear power reactor effluents as they are reported to contain free acidity and not much research has been attempted to selectively remove uranium from a number of coexisting inorganic ions present in weakly acidic to acidic solutions using IIP's [14]. Say et al. [46] selectively removed uranium using glutamic acid ion imprinted polymeric beads from weakly acidic solutions (pH 3.5) containing Fe(III), Th(IV) and Mn(II) but had a number of drawbacks like requirement of 75 min adsorption time, crucial dependence on the pH of equilibration which made the process tedious

and time consuming. Recently, Prasada Rao et al. prepared IIP based on ternary mixed ligand (UO_2^{2+}-SALO-VP) prepolymer complexes for the selective removal of uranium from dilute aqueous solutions [13].

Interest in the family of cucurbit[n]urils (CB[n], n=5–10), comprising n glycoluril units joined by pairs of methylene bridges, having a hydrophobic cavity accessible through two carbonyl-fringed portals as hosts has been increasing [47]. Cucurbiturils were developed after cyclodextrins, crown ethers and calixarenes [48-50]. The metal complexing properties of cucurbiturils have been widely investigated [51-53], particularly in the case of alkali, alkaline-earth [54-60], lanthanide cations [61] and d-block metal ions [62-66]. In the case of actinides, the crystal structures of only two compounds have been reported by Fedin et al., one having Th(IV) cation bound to three adjacent carbonyl groups complexed at each portal of CB6, and the other $[(UO_2)_4(\mu 3\text{-}O)_2(\mu 2\text{-}Cl)_4(H_2O)_6]$ [67]. CB6, having no uranium–carbonyl bond, the tetranuclear uranyl complex being only hydrogen bonded to the macrocycle [68]. These molecules exhibit wide range of applications including molecular catalysis, molecular recognition, ion channel, and supramolecular assemblies [69-71].

Recent synthesis of cucurbituril homologues (CB[*n*], n = 5, 7 and 8) has broadened the scope of the cucurbituril chemistry [72]. Thuery was the first to report complexes between uranyl ions and CB5, the heterometallic uranyl lanthanide complexes having direct uranyl-carbonyl bonds and hydrogen bonded channels [73-75]. Polynuclear complexes were also reported by him where uranyl ions were bound to two carbonyl groups from two different molecules [91-93]. CB5 is known to form capsules when capped by alkali metal or lanthanide ions, and Zn, K with different cations at its two portals [65, 73, 76-80]. In the absence of other reactants (alkali metal/lanthanide ions, Zn and K) the problem of formation of insoluble powders and/or small quantity of crystals was reported by Thuery under hydrothermal conditions [73-75].

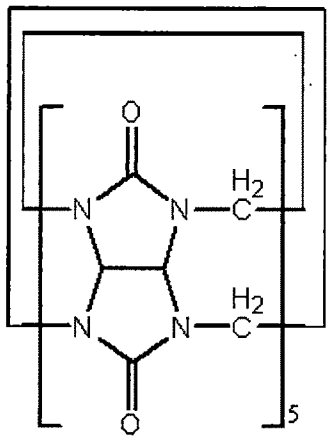

Scheme 8.2. Cucrbit[5]uril

The environment and the size of the two carbonyl fringed portals [2.4 Å] led us to believe that CB5 (Scheme 8.2) would be a perfect molecule for the complexation of uranyl ions [0.81Å] at each of its portals. Literature search prominently showed that very few of the studies have reported selective extraction and recovery of uranium using ion imprinted polymers in the acidic pH range. Our objectives were:

i) To prepare U2CB5 complex and characterize the complex by XRD, NMR, UV, IR and fluorescence studies.

ii) To explore the possibility of U2CB5 complex being a suitable monomer for the preparation of ion imprinted oligomer.

iii) Due to their structural morphology and low cost explore the possibility of the use of agro-waste palm shell powder as potential support material for the grafting of imprinted oligomer.

However, during the course of our attempt to prepare a complex of uranyl nitrate with CB5 under ambient conditions we were pleasantly surprised to get yellow crystals of U2CB5 at ambient temperature conditions, in which both the portals are closed by uranyl ions. We thus report herein the synthesis, characterization and single crystal X-ray structure analysis of (U2CB5). This monomer containing uranyl ion as the template would be further polymerised for the preparation of ion imprinted oligomer. The imprinted polymer would then be non-covalently grafted onto palm shell powder as described in scheme 8.3.

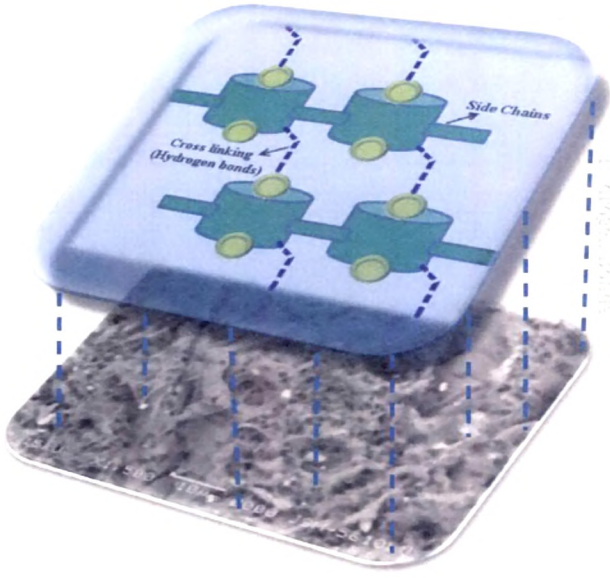

Scheme 8.3. Ion imprinted oligomer grafted on PSP

8.2. Materials.

8.2.1. Synthesis of $\{(UO_2)_2(CB5)\}(NO_3)_4 \cdot 4HNO_3 \cdot 3H_2O$ (U2CB5).

$UO_2(NO_3)_2.6H_2O$ was purchased from Sulab chemicals, HNO_3 was purchased from E-Merck and cucurbit[5]uril from Aldrich. Cucurbit[5]uril (20 mg, 0.020 mmol) was dissolved in 4.6 mL of demineralized water and 0.4 mL of HNO_3 (69% w/v) was added to it. A 10-fold excess of $UO_2(NO_3)_2 \cdot 6H_2O$ (116 mg, 0.232 mmol) was dissolved in 4.9 mL of demineralized water and 0.1 mL of HNO_3 (69% w/v) was added to it. The uranyl nitrate solution was added dropwise to cucurbituril solution with continuous stirring and was left for 24 h at 40°C under stirring conditions and the complex is readily synthesized. Light yellow color crystals of the complex U2CB5 were deposited in solution. Good quality single crystals of light yellow color could be separated within 24 h, which if left further for another 24 h resulted in crystalline material. Anal. Calcd. for $C_{30}H_{40}N_{28}O_{41}U_2$: C, 18.75; H, 2.08; N, 20.42. Found C, 18.82; H, 1.97; N, 20.54%. The observed percentage of U was found to be 12.41% (Anal. Calcd. 12.39%). 1H NMR (D_2O/HCl 300K): δ (ppm) 6.873, 8.190 (d, $-CH_2-$) and 8.073 (s, $-CH-$) for U2CB5. 13C NMR (D_2O/HCl 300K): δ (ppm) 51.13, 71.78, and 172.88 for U2CB5. Amount of water or dilution and pH of the reaction is an important part playing role for synthesizing U2CB5 as it serves as mineralizing agent as well as counter cation.

8.2.2. Synthesis of Ion Imprinted oligomer and Grafted Ion Imprinted oligomer.

U2CB5 (107 mg) was allowed to react with $K_2S_2O_8$ (418 mg)[1:15 mole ratio] in water at 85 °C for 6 h in presence of nitrogen atmosphere. After cooling to room temperature acetone vapor diffusion into the solution gave light yellow precipitates were filtered washed with acetone and dried in vacuum oven (50°C) to give hydroxylated U2CB5. Allylation was done by adding hydroxylated U2CB5 (48.2 mg) to a solution containing NaH (27.13) (60% dispersion in mineral oil in 10 mL anhydrous DMSO) in 1:20 mole ratio at 0 °C and stirred at RT for 1 h, followed by addition of alkyl bromide (0.42 mL) to this reaction mixture at 0 °C and stirred at RT for 12 h. The reaction mixture was poured into ice-water (300 mL) resulting in a light yellow solid which was washed thoroughly with water and ether, and finally dried in vacuum to obtain allyl derivative of hydroxylated U2CB5. The product was purified number of times by washing with ether or hexane to remove the unreacted alkyl bromide. Allyl derivative of hydroxylated U2CB5 is the template complexed monomer which was polymerized using free radical solution polymerization to obtain uranyl ion imprinted polymer.

About 25 mg of allyl derivative of hydroxylated U2CB5 (Monomer) in 10 mL solution of methanol along with 10 mg recrystalised AIBN (Initiator) was taken in a three neck flask at 55 °C under nitrogen atmosphere in thermostatically controlled oil bath with constant stirring for 10 h. After completion of reaction, excess methanol was distilled off under reduced pressure and traces of solvent were removed by drying under reduced pressure in vaccum oven for 12 hours. The resulting polymer was then dried to obtain ion imprinted polymer [IU2CB5]. Imprinted polymer IU2CB5 was then grafted to a lignocellulosic agrowaste, *palm shell powder (PSP)* by dry impregnation method or forced impregnation for 12h. A grafted ion imprinted polymer [PGIU2CB5] was thus obtained.

Control polymer was similarly prepared by omitting the imprint ion $(UO_2)^{2+}$ (Controlled polymer [CU2CB5] and Controlled polymer grafted to *PSP* [CPGIU2CB5]).

8.2.3. Pretreatment of Polymer to Leach the Imprint Ion.

The imprint ion $(UO_2)^{2+}$ was leached from the imprinted polymer [LIU2CB5] and grafted imprinted polymer [LPGIU2CB5] by sonication with 10 ml of 1N $HClO_4$ for 6 h. The resultant polymer material was dried in a vacuum oven at 60^0C to obtain imprinted polymer [IU2CB5]

and grafted imprinted polymer [PGIU2CB5] for possible selective extraction of $(UO_2)^{2+}$ over other metal ions.

8.3. Methods.

8.3.1. Crystallographic Studies.

A yellow single crystal of suitable size and uniform shape was selected and mounted on a glass fiber with epoxy and aligned on a Bruker SMART APEX CCD X-ray diffractometer. Intensity measurements were performed using graphite monochromated Mo Kα radiation [λ = 0.71073 Å]. Each set had a different Φ angle for the crystal, and each exposure covered a range of 0.3° in ω. A total of 2400 frames were collected with an exposure time per frame of 40 s. ω scan width of 0.3°, each for 8 s, crystal-detector distance 60 mm, collimator 0.5 mm. The data were reduced by using SAINTPLUS and a multiscan absorption correction was done using SADABS [76-78]. Structure solution and refinement were performed using SHELX-97 [79]. All non hydrogen atoms were refined anisotropically. The final cell parameters were determined using a least-squares fit to 4713 reflections. During the crystallography 25040 reflections were collected, among which 4713 unique ones were used to solve the structure with R(int) = 0.0343.

8.3.2. ^{1}H and ^{13}C NMR Spectroscopy.

High-resolution ^{1}H and ^{13}C NMR spectra were recorded using a Varian-500 spectrometer operating at 500 MHz in D_2O/HCl. The chemical shifts δ, expressed in parts per million [ppm], were referenced relative to the signal of tetramethylsilane ($Si(CH_3)_4$) at δ = 0 ppm.

8.3.3. Fluorescence Spectroscopy.

Fluorescence and absorption data were acquired for the solutions of ligand and the compound using a Jasco spectrofluorimeter quartz cell and Lamda-35 Perkin-Elmer UV−visible spectrophotometer. Excitation was achieved using 365 nm light from a Xenon lamp for the fluorescence spectroscopy. The absorption spectra are provided in the Supporting Information. Absolute emission quantum yields were determined by comparison of the integrated emission intensity with that of quinine sulfate under identical conditions such as exciting wavelength, optical density, and apparatus parameters.

8.3.4. Powder X-ray Diffraction.

Powder X-ray diffraction pattern of the samples were collected on a PHILIPS PW-1830. XRPD pattern of the ingredients was taken by holding in place on quartz plate for exposure to CuKα radiation of wavelength 1.5406 Å. The sample was analyzed at room temperature over a range of 10–70° 2θ with sampling intervals of 0.02° 2θ and scanning rate of 2°/min.

8.3.5. Infrared Spectroscopy.

Infrared spectra were obtained from single crystals of U2CB5 and oligomers using a Perkin-Elmer RX1 model FTIR spectrometer. FT-IR spectra for the crystal was obtained by first mixing with KBr and then ground in a mortar at an appropriate ratio of 1/100 for the preparation of the pellets. The resulting mixture was pressed at 10 tons for 5 min and sixteen scans with 8 cm^{-1} resolution were applied in recording spectra. The background obtained from the scan of pure KBr was automatically subtracted from the sample spectra.

8.3.6. Thermal Analysis.

The thermal behavior of the crystal as well as oligomers was evaluated by using thermo-gravimetric analyzer (TG/DTA 6300 (INCARP EXSTAR 6000), under air at a heating rate of 10 °C min^{-1} up to 450 °C. Differential Scanning Calorimetry for oligomers was obtained by using Seiko SSC 5200H Differential Scanning Calorimeter at a uniform heating rate of 10°C/min over a temperature range of 30-550°C in nitrogen atmosphere.

8.3.7. ICP Analysis of Uranium.

For the ICP analysis, the U2CB5 complex (5 mg) was dissolved in 10 mL of water. After complete dissolution, the solution was transferred to a 25 mL volumetric flask and diluted to final volume with deionized water. Five standard solutions of uranium were used to obtain calibration curves with concentrations of 1–10 mg L^{-1} prepared from a 1000 mg L^{-1} stock solution. The standards and sample were analyzed by an inductively coupled plasma atomic emission spectrophotometer (ICP-AES, Thermo Jarrel Ash, Model Trace Scan) at wavelengths of 409.014 nm.

8.3.8. Elemental Analysis (EDAX and CHN Analyzer).

Elemental analysis was carried out using a JSM5610LV instrument combined with INCA-EDX-SEM analyzer and confirmed by Perkin-Elmer 2400 CHN analyzer for the quantitative identification.

8.3.9. Gel Permeation Chromatographic Analysis.

The weight-average molecular weight (M_w), number-average molecular weight (M_n) and polydispersity index (M_w/M_n) were obtained on a Waters 150C GPC using RI detector (1000-Å HT column).

8.3.10. Scanning Electron Microscopic Analysis.

The surface morphology and topographic analysis of the adsorbent samples was examined by Scanning Electron Microscope (JEOL, Model JSM-5610LV).

8.3.11. Selectivity Studies.

The selectivity of IU2CB5, PGIU2CB5, CU2CB5, CPGIU2CB5 for uranium over other inorganic ions was determined by shaking 20 mg of polymer particles with 25 ppm of Cu^{2+}, Cd^{2+}, Zn^{2+}, Cr^{6+}, Fe^{3+}, Cs^{+} and U^{6+} present in 10 mL of deionized water at pH1 adjusted using HNO_3. The selectivity coefficient ($S\ UO_2^{2+}/M^{n+}$) is defined as

$$S_{UO_2^{2+}/M^{n+}} = \frac{D_{UO_2^{2+}}}{D_{M^{n+}}}$$

where DUO_2^{2+} and DM^{n+} are the distribution ratios of the uranyl ion and other inorganic species, respectively, with polymer particles (CU2CB5 or IU2CB5). These distribution ratios were calculated using the formula

$$D_{M^{n+}} = \frac{C^{i}_{M^{n+}} - C^{f}_{M^{n+}}}{C^{f}_{M^{n+}}} \times \frac{v}{m}$$

where $C_i\ M^{n+}$ and $C_f\ M^{n+}$ are the concentrations of inorganic ions in aqueous phase before and after extraction, v is the volume of the solution, and m is the mass of the polymer. The percent extraction ($\%E$) of inorganic ion is defined as

$$\%E = \frac{C^{i}_{M^{n+}} - C^{f}_{M^{n+}}}{C^{i}_{M^{n+}}} \times 100$$

8.4. Result and discussion

8.4.1. Structural Characteristics for Complex.

8.4.1.1. ***Crystal Structure.*** The title compound $\{(UO_2)_2(CB5)\}(NO_3)_4 \cdot 4HNO_3 \cdot 3H_2O$ (U2CB5) crystallizes in monoclinic system with space group of *C*2/*c*. The asymmetric unit in the crystal structure of U2CB5 is composed of half of the moiety with four units of nitrate anion (two for charge compensation and other two for lattice HNO_3 molecules) and three lattice water molecules. Coordination complexes having two uranyl ions in the same molecular unit to form the internal complex are extremely rare and exhibit interesting properties. But here, in contrast to the reported results we are presenting the first internal complex of uranyl nitrate and cucurbit[5]uril under normal bench conditions.

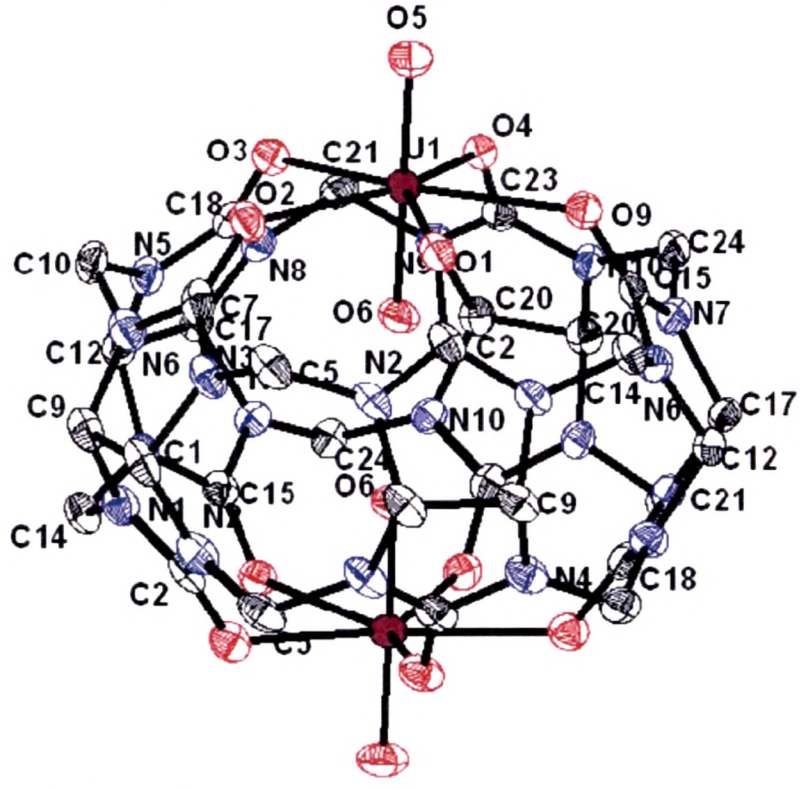

Figure 8.1. Oak Ridge thermal ellipsiodal diagram of the U2CB5 with 40% probability (Hydrogens, counteranion and solvent water molecules are omitted for clarity): Color code: C, gray; O, red: N, blue;.

The full molecule of the U2CB5 as shown in Figure 8.1 is a biuranyl complex with cucurbit[5]uril (CB5) and crystallographic data with structural refinement parameters are provided in Table 8.2.

Table 8.2. Crystallographic Data and Structural Refinement

Entry	U2CB5
Formula	$C_{30}H_{30}N_{28}O_{41}U_2$
Volume	1914.88
Crystal system	Monoclinic
Space group	C2/c
a/Å	15.0886 (15)
b/Å	14.5869 (14)
c/Å	24.889 (2)
β /deg	93.6340(10)
U/Å^3	5340.6 (9)
Z	4
F(000)	3672
ρ_{cal}/ Mg m^{-3}	2.382
Crystal size(mm^3)	0.36 x 0.22 x 0.14
Completeness to θ =25.0	100 %
Theta range for data collection(deg)	1.68 to 25.0
Reflections collected/ unique	25040/ 4713 [R(int) = 0.0343]
$R_1(F^2_0)$ [I > 2 σ(I)]	0.0349
wR_2 (F^2_0) [I > 2 σ(I)]	0.0957
$R_1(F^2_0)$ (all data)	0.0395
wR_2 (F^2_0) (all data)	0.0992
Largest diff. peak and hole(Å^{-3})	1.323 and -1.427

Here, uranyl cations fit into both open portals of CB5 molecule. The U–O bond lengths with the five carbonyls of CB5 is in the range of 2.413(4)-2.454(4) Å while in the case of pendant uranyl oxygens it is 1.748(5)–1.759(5) Å. The hydrogen bonding environment around $\{(UO_2)_2(CB5)\}^{4-}$ is quiet interesting, which is shown in the Figure 8.2 where the length of C–H···O is 2.40 to 2.80 Å. The hydrogen bonding distances and angles are represented in Table 8.3.

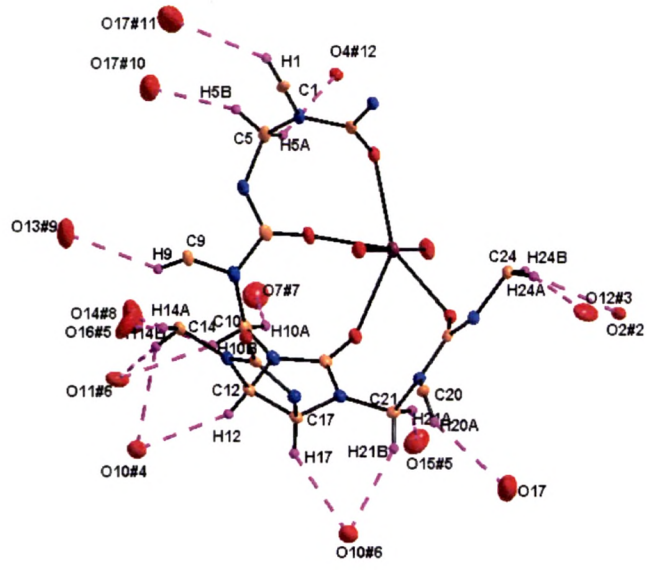

Figure 8.2. Hydrogen bonding situation around the asymmetric unit of the U2CB5: Color code: C, grey; O, red: N, blue; H, purple.

Table 8.3. Hydrogen bonds for U2CB5 [Å and deg.]

D-H...A	d(D-H)	d(H...A)	d(D...A)	<(DHA)
C(24)-H(24A)...O(2)#2	0.97	2.74	3.460(7)	131.3
C(24)-H(24B)...O(12)#3	0.97	2.39	3.324(8)	162.4
C(20)-H(20A)...O(17)	0.85(6)	2.51(6)	3.275(12)	150(5)
C(21)-H(21B)...O(10)#4	0.97	2.48	3.353(8)	149.4
C(21)-H(21A)...O(15)#5	0.97	2.45	3.297(9)	146
C(17)-H(17)...O(10)#4	0.92(5)	2.47(5)	3.248(9)	142(4)
C(12)-H(12)...O(10)#6	0.87(7)	2.54(7)	3.313(8)	148(5)
C(14)-H(14B)...O(10)#6	0.97	2.81	3.591(9)	138.5
C(14)-H(14A)...O(16)#5	0.97	2.49	3.460(9)	176.6
C(10)-H(10A)...O(7)#7	0.97	2.63	3.429(11)	139.6
C(10)-H(10B)...O(14)#8	0.97	2.89	3.586(10)	129.4
C(10)-H(10B)...O(11)#6	0.97	2.67	3.565(9)	153.2
C(14)-H(14B)...O(11)#6	0.97	2.39	3.331(9)	162.4
C(9)-H(9)...O(13)#9	0.94(7)	2.53(6)	3.226(9)	131(5)
C(5)-H(5B)...O(17)#10	0.97	2.4	3.285(12)	150.7
C(1)-H(1)...O(17)#11	0.89(6)	2.68(6)	3.416(13)	141(5)
C(5)-H(5A)...O(4)#12	0.97	2.47	3.257(7)	138.6

Symmetry transformations used to generate equivalent atoms: #1 -x,y,-z+1/2 #2 -x+1/2,y+1/2,-z+1/2 #3 x-1,y,z #4 -x+1,y,-z+1/2 #5 x-1/2,y-1/2,z #6 x-1,-y+1,z+1/2 #7 -x+1/2,-y+1/2,-z+1 #8 -x+1,-y+1,-z+1 #9 x-1,y-1,z #10 x,y-1,z #11 -x,y-1,-z+1/2 #12 -x+1/2,y-1/2,-z+1/2

The environment of nitrate anion around $\{(UO_2)_2(CB5)\}^{4-}$ looking like a wheel is shown in Figure 8.3, C–H···O interaction being responsible for the whole architecture.

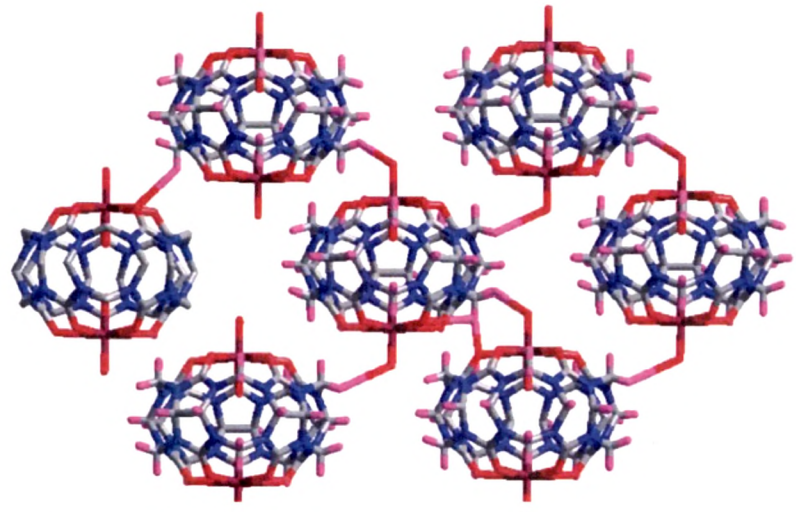

Figure 8.3. C–H···O interaction

Extensive O–H···O interaction has been found in the crystal structure of U2CB5, which leads to a 2-dimensional network as represented in Figure 8.4.

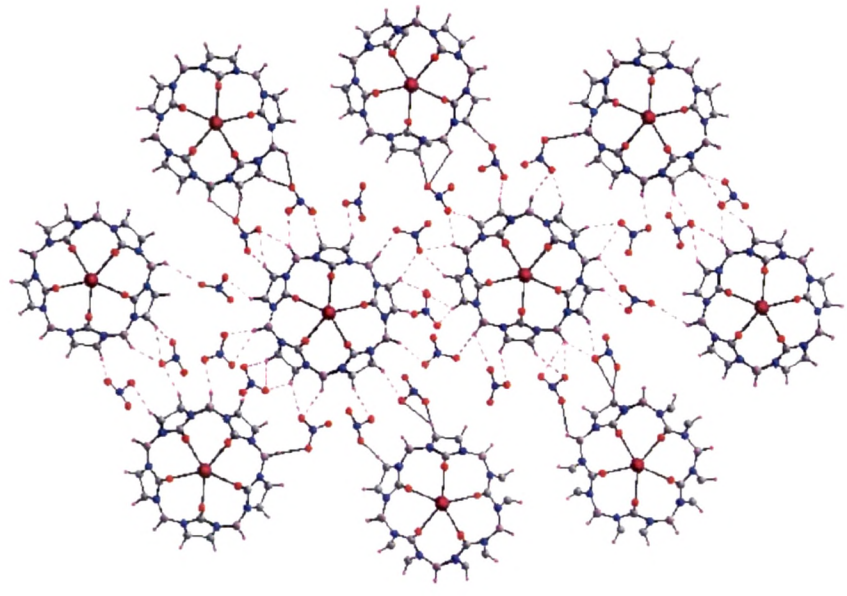

Figure 8.4. Environment of nitrate ions

The water molecules are involved in both intra- and intermolecular hydrogen bonding. The distance between the uranium atoms is 6.079 Å, and the separation between the inner oxo

groups is 2.562 Å. The water molecules are located in the intermolecular spaces. The uranyl ion is perpendicular to the O plane, with an angle of ~94° with the normal to the plane and the uranium environment is thus a regular pentagonal bipyramid.

8.4.1.2. ***Powder- X-Ray Diffraction.*** The phase purity of U2CB5 was confirmed by XRPD patterns (Figure 8.5 a–c). Peak positions of the experimental and simulated spectra are in good agreement with each other indicating overall homogeneity of the samples and showing that single crystal and bulk properties remains the same.

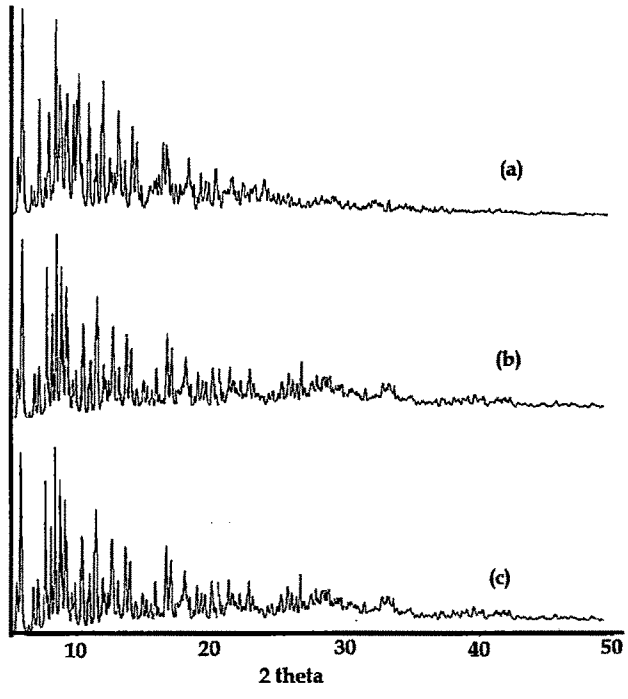

Figure 8.5. (a) Simulated pattern of U2CB5 (b) Powder diffraction pattern of U2CB5 Single crystal (c.) Powder diffraction pattern of U2CB5 crystalline material

The unit cell parameters from the powder data were found to be in good agreement with that of single crystal. X-ray powder diffraction patterns showed numerous reflections in the low to high angle regions, indicative of crystalline phases. The high intensity Bragg reflections (7.2, 8.7, 12.6, 15.4, 16.9, 18.0, 18.6, 19.9, 20.9, 21.7 Å) are likely due to the strongly scattering uranyl cations [12, 80].

8.4.1.3. ***^{1}H and ^{13}C Nuclear Magnetic Resonance.*** The ^{1}H decoupled NMR spectrum showed upfield shifting of the signals due to deshielding of protons after complexation. Two doublets ($-CH_2-$) and a singlet ($-CH-$) along with a very broad signal (D_2O) appeared at ~4.2 and 5.6 (d), ~5.4 (s) and ~4.7 ppm for CB5 which shifted upfield to ~6.9 and 8.2 (d), 8.1 (s), and 7.3 ppm, respectively, after complexation with uranium (Figure 8.6). The ^{13}C NMR spectrum (Figure 8.6) showed chemical shifts at 49.91, 68.95, and 156.23 ppm, which can be attributed to $N-CH_2-N$, $N-CH-N$, and $-C=O$ groups, respectively, in CB5. While there were small changes in chemical shifts attributed to $N-CH_2-N$ and $N-CH-N$ in U2CB5, the chemical shift of $-C=O$ at 156.23 ppm shifted downfield to 172.88 ppm. This probably indicates the formation of covalent bond between highly electronegative uranyl ion to the carbonyl moiety of CB5.

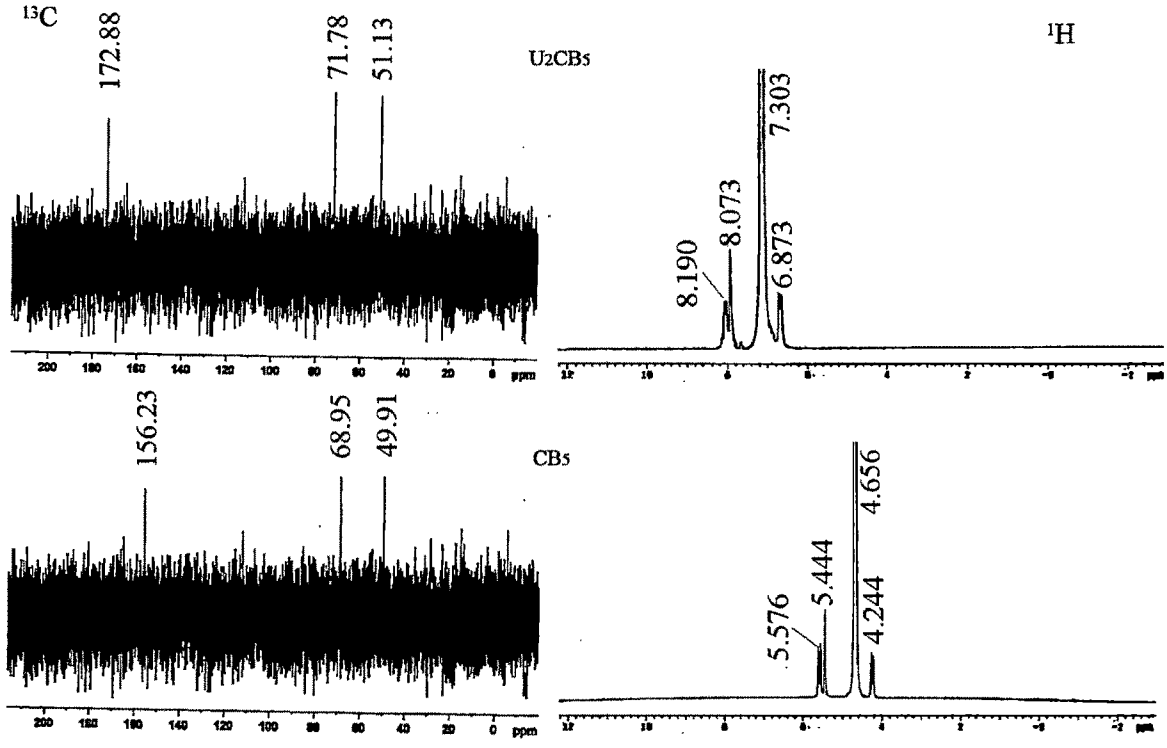

Figure 8.6. ^{1}H and ^{13}C spectra for CB5 and U2CB5

8.4.1.4. ***Thermal Analysis.*** The DTA curve of CB5 (Table 8.4 and Figure 8.7) shows an endothermic transition in the temperature interval 67.704–151.24 °C, which corresponds to a mass loss of 9.13% in the TG curve. This weight loss corresponds to the loss of 4.6 lattice water molecules. CB5 loses most of its weight (52%) around 400 °C.

Table 8.4. Thermal analysis for CB5 and U2CB5

	CB5		U2CB5	
	Temperature	% weight loss	Temperature	% weight loss
TGA Analysis	21.618 - 67.704	8.699	38.761 – 85.051	3.331
	67.704 - 151.24	9.13	85.051 - 137.09	2.703
			137.09 - 172.243	2.391
	151.24 - 332.932	1.763	172.243 - 270.619	7.015
			270.619 - 355.758	16.183
	332.932 - 547.72	52.391	355.758 - 549.087	8.776
Total % Weight loss	71.983		40.399	

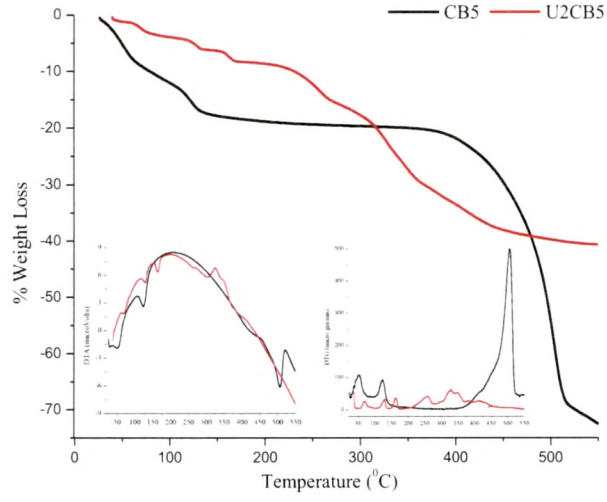

Figure 8.7. Thermal analysis of CB5 and U2CB5

After complexing, DTA curve of U2CB5 showed an endothermic transition in the temperature interval 85.051−172.243 °C. This corresponds to a mass loss of 5.094% in the TG curve equivalent to 5.6 lattice water molecules. An exothermic transition in the temperature interval 270.619−355.758 °C, corresponding to a mass loss of 16.183% in the TG curve occurs due to decomposition of ligand and formation of UO_3 [81]. Thus the weight loss is less in U2CB5 around 400 °C in contrast to CB5, but it overlaps with the ligand decomposition and gives a continuous weight loss until the final product UO_3 is formed at about 450 °C.

8.4.1.5. ***Fourier Transform Infra Red Spectroscopic Analysis.*** The selected vibrations from FT-IR spectra of CB5 and U2CB5 with the suggested assignments, are listed in Table 8.5. The very strong and broad bands found at ~3439 and 3423 cm^{-1} and sharp bands at 1636 cm^{-1} in the spectra are consistent with the presence of water molecules in the ligand and complex, also supported by the single crystal XRD.

Table 8.5. FTIR frequencies for ligand and complexes

	CB5	U2CB5
-C=O Stretching	1738	1695
-CH Stretching & bending	3002	3020
	2941	2924
	1485	2830
	1382	1381
$-NO_3$ stretching	-	1766
Stretching & bending of H_2O	3439	3423
	1636	1653
U-O Bending	-	579, 480 , 445, 948, 859

Frequencies of the stretching and bending vibrations of the C–C, C–N, and C–H groups of cucurbituril were also observed. The IR spectra of the complex show strong and weak absorption bands between 950 and 850 cm^{-1}, and weak bands in the region 580–450 cm^{-1} (Figure 8.8).

The bands at about 948, 579, and ~480 cm^{-1} are assigned to the asymmetric U–O stretching modes and those at about 859 and 445 cm^{-1} to the symmetric U–O stretching modes of the uranyl moiety [82]. The strong absorption band observed at 1766 cm^{-1} may be assigned to the nitrate. Infrared spectral studies as well as X-ray structural determinations have established that in the complex, nitrate groups are acting as counterions. Stretching frequencies in the complex is significantly shifted toward lower wave-numbers Table 8.5 as a result of oxygen–uranium coordination. The formation of a U–O bond, leads to a decrease in the π character of the C=O bond.

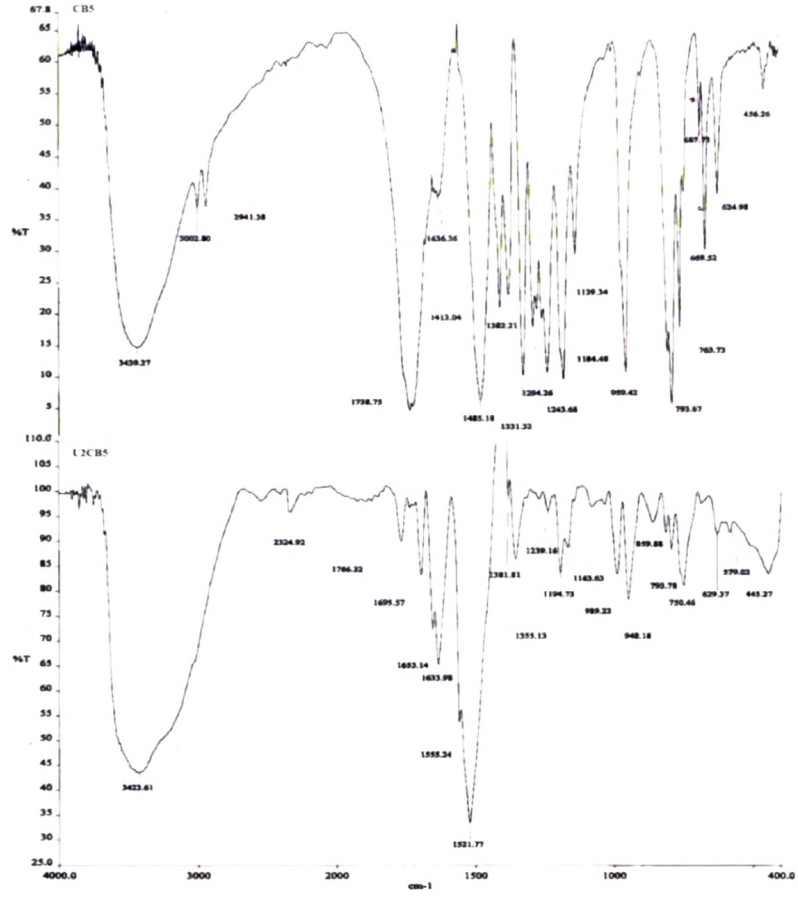

Figure 8.8. FTIR spectra for the CB5 and U2CB5

8.4.1.6. ***Fluorescence Spectroscopy.*** Uranyl nitrate was found to exhibit the typical greenish-yellow fluorescence with vibronic transitions [107-109] of uranyl ion when excited at 266 nm Figure 8.9.

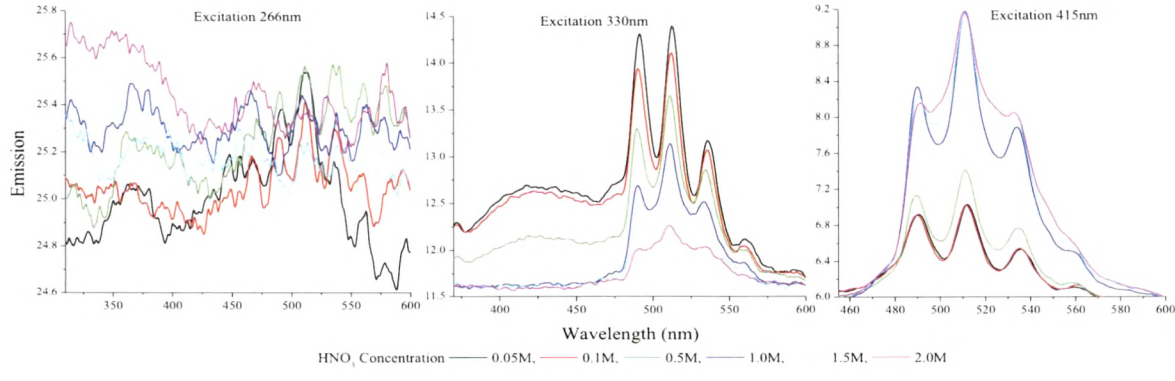

Figure 8.9. Emission spectra of uranyl nitrate with variation in excitation wavelength and HNO_3 concentration

The acidity of the medium seemed to play a vital role in the characterisitics of the emission spectra of uranyl nitrate (Figure 8.10) [83]. Change in excitation wavelength from 266 to 330 nm to 415 nm led to an increase in resolution of the individual vibronic transitions with decrease in the intensity of emission (Figure 8.10 (inset)).

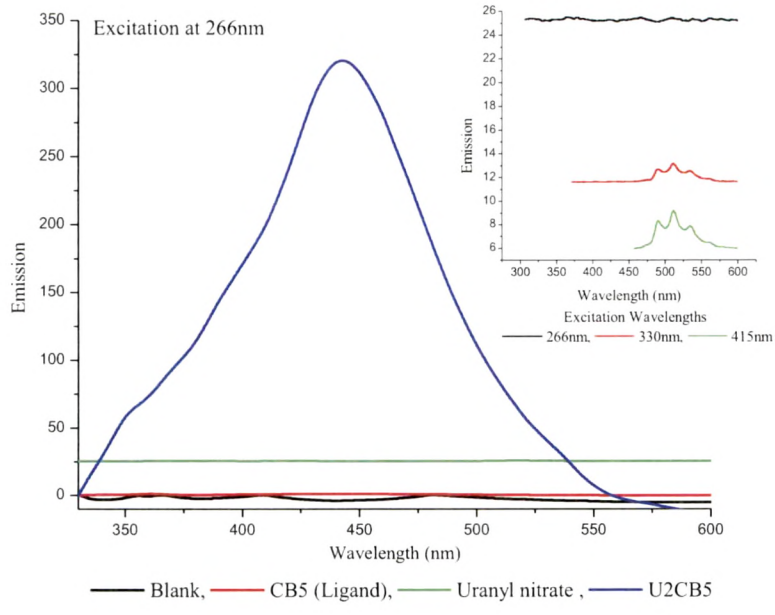

Figure 8.10. Emission spectra of CB5, Uranyl nitrate and U2CB5 excited at 266nm and emission intensity measured at 432nm, inset emission intensities of uranyl nitrate excited at 266nm, 330nm and 415nm

Hence, emission for U2CB5 was measured in ~1.0 M HNO_3 by excitation at 266 nm at room temperature where maximum emission intensity and a well resolved spectrum was observed for uranyl nitrate at 516 nm. The fluorescence intensity of uranyl ion increased remarkably (25.53−319), and the emission peak gradually shifted from 516 to 432 nm upon complexation with CB5 (Figure 8.10). The bonding of uranium to carbonyl groups and hence formation of complex with a macrocycle like CB5 suppresses the various vibrational modes present in uranyl ion [84]. Furthermore the presence of two uranyl ions bound to CB5 could also be responsible for enhanced fluorescence. Thus the formation of inclusion complex of uranyl ion with CB5, led to a hypsochromic shift with fluorescence enhancement. Increase in excitation wavelength from 266 to 330 to 415 nm led to an increase in resolution of the individual vibronic transitions while at the same time decrease in the intensity of emission was observed. The effect

of acidity of the medium was also investigated by performing the experiments in 0.05, 0.10, 0.50, 1.00, 1.50, 2.0 M nitric acid. The spectra obtained by excitation at 330 nm were found to be of high emission intensities and well resolved in <1 M nitric acid, while they were broad, unresolved and of lesser intensity in media containing higher concentration of nitric acid. On the other hand, the spectra obtained by excitation at 415 nm in <1 M nitric acid are found to be well resolved with maxima at 516 nm. When the concentration is increased above 1 M the peak at 518 nm is prominent with increased intensity while the other peaks appear only as shoulders. The extinction coefficient, however was much higher and the spectra were better structured for the 330 nm excitation wavelength in comparison with the 415 nm excitation wavelength. Thus the formation of inclusion complex of uranyl ion with CB5, led to a hypsochromic/blue shift with a fluorescence enhancement.

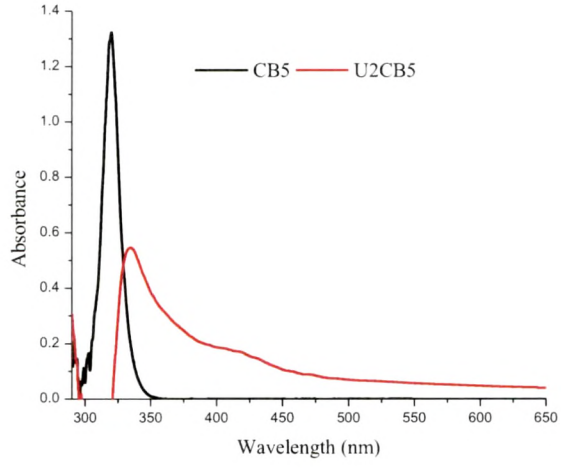

Figure 8.11. UV-Visible absorption spectra of CB5 and U2CB5

Absorption spectral characteristics of U2CB5 showed a bathochromic shift of the charge transfer band (uranium to oxygen) from 319 to 334 nm and a less intense broad shoulder in the visible region at 420 nm (Figure 8.11). The broad character of the U2CB5 could be due to electron transfer involving π- bond contribution (d $\rightarrow$ f transition).

The luminescence spectrum of a solution of uranyl nitrate (0.15 M, pH 1.3) is shown in Figure 8.11. The quantum yield of uranyl nitrate has been previously determined using fluorescein as reference, since its emission spectrum closely overlaps with that of the uranyl ion. However, fluorescein is reported to have some drawbacks as fluorescent standard because of its

instability in solution and the dependence of its emission spectrum on pH [85]. We have, thus, determined the luminescence quantum yield for uranyl nitrate solution using, quinine sulfate in 1 M sulfuric acid (quantum yield = 0.546) [86] at excitation wavelength 282 nm. Luminescence quantum yields of 2.7×10^{-3} and 0.75 were obtained for uranyl nitrate and U2CB5 respectively using quinine sulfate as standard. A quantum yield of 0.75 was also reported for the complex $[UO_2(bipyO_2)H_2O](ClO_4)_2$ by Hnatejko et al. [87].

8.4.2. Structural Characteristics for Oligomer.

8.4.2.1. ***Gel Permeation Chromatographic Analysis.*** The molecular weight of the prepared oligomer was determined using size exclusion chromatography (Figure 8.12) and it is clearly seen that the oligomer was of low degree of polymerization with a molecular weight of 11968 dalton and poly-dispersity index of 1.783.

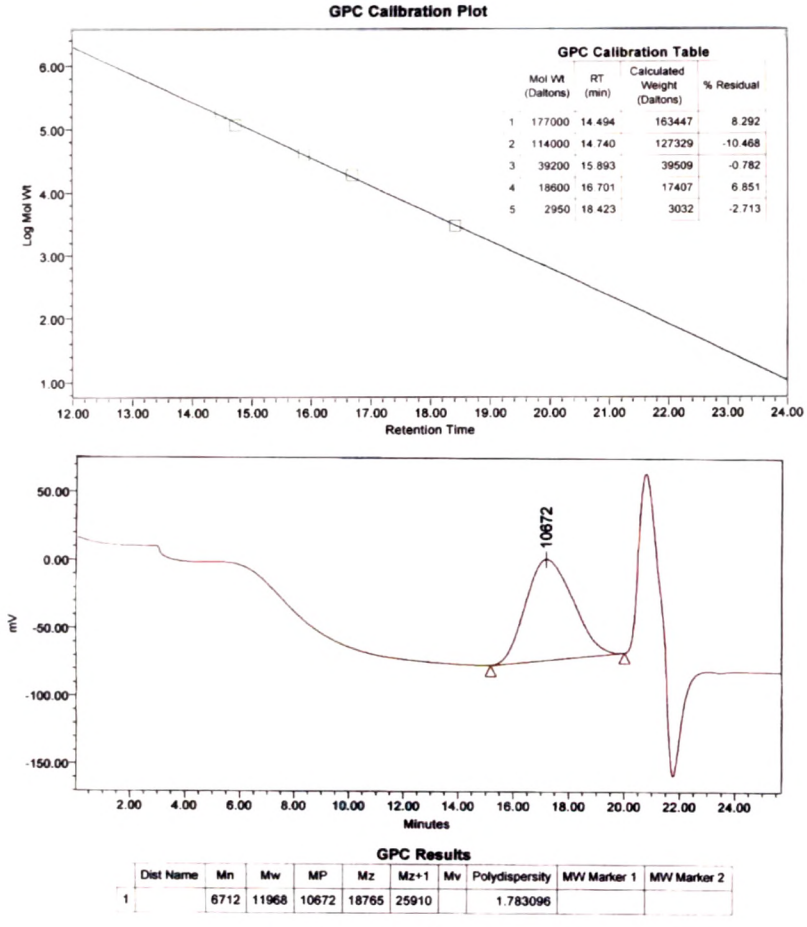

Figure 8.12. GPC calibration and experimental results for IU2CB5

8.4.2.2. *Thermal Analysis.* The TGA curves of IU2CB[5], PGIU2CB[5], LIU2CB[5] and LPGIU2CB[5] (Table 8.6 and Figure 8.13) show gradual loss of mass in the temperature range 28-165^{0}C which corresponds to a loss of adsorbed water molecules.

Table 8.6. Thermal analysis of IU2CB[5], PGIU2CB[5], LIU2CB[5] and LPGIU2CB[5]

IU2CB[5]		LIU2CB[5]		PGIU2CB[5]		LPGIU2CB[5]	
Temperature (^{0}C)	% weight loss	Temperature (^{0}C)	% weight loss	Temperature (^{0}C)	% weight loss	Temperature (^{0}C)	% weight loss
34.64-90.97	1.93	28.07–72.71	9.21	34.76-107.60	2.21	33.81-144.5	3.11
90.97-162.31	3.93	72.71-142.43	8.44	107.60-328.18	14.03	144.5-265.09	4.51
162.31-329.95	35.24	142.43–354.26	2.82				
329.95-559.58	10.99	354.26-516.57	48.84	328.18-519.88	14.30	265.09-486.85	14.10
		516.57-557.96	4.49	519.88-559.58	1.96	486.85-560.12	2.61
Total % Weight loss							
52.44		73.21		32.519		24.33	

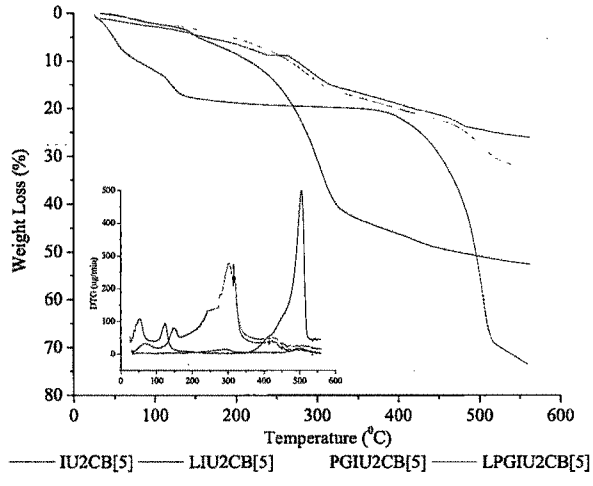

Figure 8.13. Thermal analysis TGA and DTG of IU2CB[5], PGIU2CB[5], LIU2CB[5] and LPGIU2CB[5]

IU2CB[5] and PGIU2CB[5] showed a continuous weight loss upto 450^{0}C in the TGA curve due to decomposition of oligomer [88]. After formation of stable UO_3 there is not much change in weight of the oligomer whereas leached oligomer showed a sharp decrease in weight loss till 550^{0}C. It can be interpreted that PGIU2CB[5] (32.52 % mass loss) is more stable than IU2CB[5] (52.44 % mass loss) while LIU2CB[5] (73.21 % mass loss) was found to be least stable. DSC analysis presented the glass transition temperatures for IU2CB[5], PGIU2CB[5], LIU2CB[5] and LPGIU2CB[5] at 105.41, 98.77, 102.18 and 88.2 ^{0}C showing the polymeric nature (Figure 8.14). The lower T_g of PGIU2CB[5] suggests the absence of chemical interactions between the oligomer and PSP.

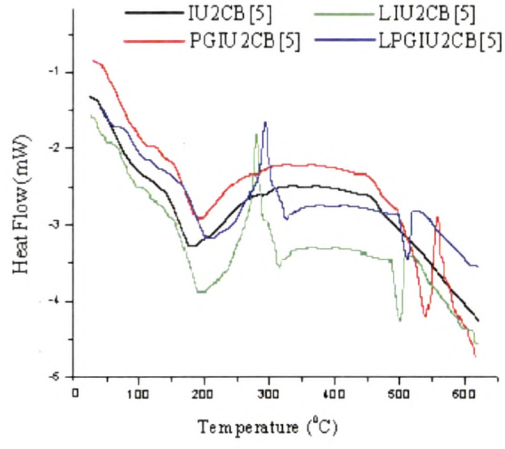

Figure 8.14. DSC analysis of IU2CB[5], PGIU2CB[5], LIU2CB[5] and LPGIU2CB[5]

8.4.2.3. ***Scanning Electron Microscopic Analysis.*** The scanning electron micrographs are shown in Figure 8.15. The micrograph for IU2CB[5] showed the presence of some non-charged species and an agglomerate of amorphous particles could be seen anchored on the surface of PSP in PGIU2CB[5]. The oligomers were monolithic in nature. After leaching LIU2CB[5] showed very bright images which could probably be due to less electron density and amorphous nature of the oligomer in the absence of uranium. The presence of holes strongly indicated that a template imprint was formed.

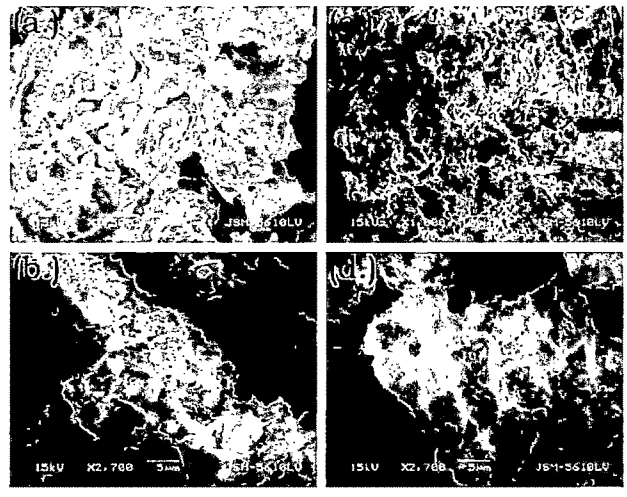

Figure 8.15. Scanning Electron Micrographs (a.)IU2CB[5] (b.)PGIU2CB[5] (c.)LIU2CB[5] and (d.) LPGIU2CB[5]

8.4.2.4. ***Fourier Transform Infra Red Spectroscopic Analysis.*** The selected infrared bands of IU2CB[5], PGIU2CB[5], LIU2CB[5] and LPGIU2CB[5] with the suggested assignments (frequency in cm^{-1}), are listed in Table 8.7.

Table 8.7. FTIR spectral assignments (frequency in cm^{-1})

Functional groups	CB5/ U2CB[5]	CU2CB[5]/ IU2CB[5]	LIU2CB [5]/ LPGIU2CB[5]	PSP	CPGU2CB[5]/ PGIU2CB[5]
-C=O Stretch	1738/ 1766	1745/ 1759	1750/ 1732	1732	1742/ 1764
-CH Stretch & bend	3002, 2941, 1485, 1382/ 3020, 2924, 2830, 1381	2989, 2915, 2827, 1380/ 2930, 2915, 2827, 1380	2994, 2932, 2825, 1390/ 2959, 2895, 1454, 1373	2959, 2895 1454, 1430 1373	2991, 2940, 2833, 1390/ 2991, 2928, 2832, 1385
Stretch & bend of H_2O	3439, 1636/ 3445, 1695, 1653	3429, 1680/ 3396, 1692	3401, 1642, 1670/ 3391, 1648	1648	3402, 1640, 1670/ 3402, 1639, 1669
-OH stretch & bend (1^0 alcohol)	-/ -	-/ -	-/ 3391	3361	-/ 3402
-C-O- bend	-/ -	1044/ 1256, 1044	1235, 1052/ 1254, 1059	1250, 1049	1051/ 1215, 1057
$CH=CH_2$ bend	-/ -	-/ -	-/ -	-	-/ -
-C-H bend	959, 793, 630/ 964, 788, 624	-/ -	964, 788, 624/ -	893, 809	-/ 962, 878, ~710
U-O Stretch	-/ 579, 480, 445, 948, 859	-/ 580, 481, 448, 951, 864	-/ -	-	-/ 583, 483, 450, 952, 859

The very strong and broad band found at ca. ~3440cm^{-1} and sharp bands at ~1636, ~1695 cm^{-1} in the spectra are consistent with the presence of water molecules in all the samples. All the reported frequencies of the stretching and bending vibrations of cucurbituril were also observed confirming that there is no adverse affect on cucurbituril after complexation and during polymerisation and grafting. Furthermore, the bands at about ~948, ~579 and ~480 cm^{-1} assigned to the asymmetric U-O stretching modes and at about 859.88 and 445.27 cm^{-1} to the symmetric U–O stretching modes of the uranyl moiety [81] were present in all the intermediates as well as imprinted and grafted oligomer but were found to be absent in leached and control oligomer. The IR spectra of IU2CB[5], LIU2CB[5] and PGIU2CB[5], LPGIU2CB[5] respectively were similar, indicating that the leaching process was not affecting the oligomer network and also that cucurbituril remains intact even after leaching. Leaching, left cavities with a predefined cucurbituril array that is able to selectively recognize and rebind the uranyl ion.

8.4.3. Uranium Selectivity Studies.

The distribution ratio, selectivity coefficients and imprinting coefficient of uranyl ion with respect to metal ions like Cu^{2+}, Cd^{2+}, Zn^{2+}, Fe^{3+}, Cs^{+} and Cr^{6+} using CU2CB[5], CPGU2CB[5], IU2CB[5] and PGU2CB[5] are shown in Table 8.8, Table 8.9 and comparison with reported literature is provided in 8.10.

Table 8.8. Imprinting Coefficient

k'	CU2CB[5]	IU2CB[5]	CPGU2CB[5]	PGIU2CB[5]
	1st adsorption		2nd Adsorption	
Cu	4729.005	1652.276	11321.300	2712.278
Cd	8347.820	2344.075	7518.860	2426.503
Zn	4612.201	1295.023	4380.860	1326.225
Cr	3029.618	667.289	3109.912	860.125
Fe	987.349	754.706	967.029	824.912
Cs	555.048	181.451	484.932	207.130

Table 8.9. Distribution ratio and selectivity coefficient

Distribution ratio K_d/ Selectivity Coefficient k								
	CU2CB[5]	IU2CB[5]	CPGU2CB[5]	PGIU2CB[5]	CU2CB[5]	IU2CB[5]	CPGU2CB[5]	PGIU2CB[5]
	1st adsorption				2nd Adsorption			
Cu	0.181/ 0.554	0.008/ 2619	0.164/ 2.142	0.007/ 3539	0.171/ 0.593	0.003/ 6710	0.156/ 2.079	0.004/ 5640
Cd	0.431/ 0.232	0.011/ 1934	0.412/ 0.851	0.012/ 1994	0.408/ 0.248	0.010/ 1865	0.379/ 0.855	0.011/ 2074
Zn	0.328/ 0.305	0.015/ 1406	0.205/ 1.714	0.011/ 2219	0.305/ 0.332	0.013/ 1453	0.192/ 1.691	0.010/ 2242
Cr	0.263/ 0.380	0.018/ 1152	0.145/ 2.417	0.015/ 1612	0.251/ 0.403	0.015/ 1254	0.149/ 2.168	0.012/ 1865
Fe	0.379/ 0.263	0.081/ 260	0.460/ 0.763	0.042/ 576	0.318/ 0.319	0.061/ 309	0.395/ 0.820	0.033/ 676
Cs	0.239/ 0.417	0.091/ 232	0.167/ 2.107	0.063/ 383	0.206/ 0.492	0.079/ 238	0.139/ 2.332	0.047/ 483
U	0.099/ -	21.124/ -	0.351/ -	24/ -	0.101/ -	18/ -	0.324/ -	22/ -

The selectivity coefficients (K) of uranyl ion over Cu^{2+}, Cr^{6+}, Zn^{2+}, Cd^{2+} ranged from >103 to $3.82x10^2$ over Fe^{3+} and Cs^+. The selectivity coefficients for CPGU2CB[5] were greater by 2 to 8 fold as compared to CU2CB[5]. The selectivity coefficient of PGIU2CB[5] increased $7.7x\ 10^2$ fold to $1.6x10^3$ fold over CPGU2CB[5] owing to the size and shape specific cavities created in PGIU2CB[5] unlike CPGU2CB[5]. Similarly the selectivity coefficient of IU2CB[5] was $5.5x10^2$ to $4.7\ x10^3$ times higher over CU2CB[5]. This observation is attributed to imprinting effect. Interestingly the selectivity coefficient increased during second cycle of adsorption by 1.2 to 1.5 times in presence of Fe^{3+}, Cs^+, Cu^{2+} and Cd^{2+} for PGIU2CB[5] which could be probably due to improved memory effect. This improvement was not observed in case of IU2CB[5] in presence of other metal ions except copper while in CU2CB[5] it was not observed in presence of all the metal ions under study. Based on the results shown in Table 8.10, it is clear that U(VI) can be removed selectively from several inorganic species present in dilute aqueous solutions and it is evident that the prepared imprinted oligomer's efficiency is comparable to those reported in literature. Furthermore the material also shows selectivity towards uranium over iron which is a major constituent in front end nuclear industry effluents.

Table 8.10. Comparison with IIP's reported in literature

Ion	Wt. of IIP (mg)	Concentration	K	(k')	Reference
Salo & Vinyl Pyrindine					
Cu^{2+}	100	100 µg/L	1650	157	[18]
Zn^{2+}			825	412	
Fe^{2+}			582	529	
CrO_4^{2-}			9900	309	
Styrene & DVB					
Cu^{2+}	100	0.5 mg/L	277	-	[12]
Zn^{2+}			219	-	
Piroxicam					
Cu^{2+}	100	15 µg/L	104	-	[17]
Zn^{2+}			96	-	
Fe^{3+}			43	-	
Cu^{2+}	100	20 mg/L	130	2.7	[13]
Zn^{2+}			630	1.7	
Fe^{3+}			25	4.9	
Cu^{2+}	100	20 mg/L	1500	6.8	[13]
Zn^{2+}			9500	20.2	
Fe^{3+}			200	1.6	
Cu^{2+}	20	25 mg/L	3539	1652	This work
Zn^{2+}			2219	1295	
Fe^{2+}			576	754	
CrO_4^{2-}			1613	667	

8.5. Conclusions.

Uranyl complex reported herein is the first molecular capsule ever reported with CB5 where both the portals are closed by uranyl ions bound to five oxygen donors obtained in a single step under ambient conditions. Another novelty is the fluorescence study of U2CB5 molecular capsule under ambient conditions which may provide new avenues for research in actinide sensing and molecular recognition. A uranyl complexed cucurbituril oligomer grafted noncovalently led to a rigid, cost-effective ion imprinting oligomer selective for uranium in acidic conditions. Neither this approach nor any other method for synthesis of ion imprinting oligomers based on cucurbiturils has been reported. The prepared imprinted oligomer using cucurbituril, with high imprinting coefficients especially over iron and retention capacity offer possible application towards removal of uranium from front end nuclear effluents.

Literature Cited.

1. G. Wulff. *Angew. Chem., Int. Ed. Engl.* **1995**, *34*, 1812.
2. N. Masquee, R. M. Marcee, F. Borrull, *Trends Anal. Chem.* **2001**, *20*, 477.
3. M . Shamsipur, J. Fasihi, K.Ashtari, *Anal. Chem.* **2007**, *79*, 7116.
4. X. Zhang, C. Ding, H. Liu, L. Liu, C. Zhao, *Toxicology* **2011**, *286*, 75.
5. G. D. Saunders, S. P. Foxon, P. H. Walton, M. J. Joyce, S. N. Port, *Chem. Commun.* **2000**, 273.
6. S. Dai, Y. S. Shin, C. E. Barnes, L. M. Toth, *Chem. Mater.* **1997**, *9*, 2521.
7. M. Kruppa, B. Konig, *Chem. Rev.* **2006**, *106*, 3520.
8. J. M. Gladis, T. P. Rao, *Microchim. Acta* **2004**, *146*, 251.
9. J. M. Gladis, T. P. Rao, *Anal. Lett.* **2003**, *36*, 2107.
10. P. Metilda, J. M. Gladis, T. P. Rao, *Anal. Chim. Acta* **2004**, *512*, 63.
11. C. F. Poole, *Trends Anal. Chem.* **2003**, *22*, 362.
12. S. J. Ahmadi, O. N. Kalkhoran, S. S. Arani, *J. Hazard. Mater.* **2010**, *175*, 193.
13. P. Metilda, J. M. Gladis, G. Venkateswaran, T. P. Rao, *Anal. Chim. Acta* **2007**, *587*, 263.
14. C. R. Preetha, J. M. Gladis, T. P. Rao, *Environ. Sci. Technol.* **2006**, *40*, 3070.
15. Y. Liu, X. Cao, R. Hua, Y. Wang, Y. Liu, C. Pang, Y. Wang, *Hydrometallurgy* **2010**, *104*, 150.
16. P. Metilda, K. Prasad, R. Kala, J. M. Gladis, T. P. Rao, G. R. K. Naidu, *Anal. Chim. Acta* **2007**, *582*, 147.
17. S. Sadeghi, A. A. Mofrad, *React. Funct. Polym.* **2007**, *67*, 966.
18. D. K. Singh, S. Mishra, *Anal. Chim. Acta* **2009**, *644*, 42.
19. T. E. Milja, K. P. Prathish, T. P. Rao, *J. Hazard. Mat.* **2011**, *188*, 384.
20. J. Fasihi, S. A. Alahyari,; M. Shamsipur, H. Sharghi, A. Charkhi, *React. Funct. Polym.* **2011**, *71*, 803.
21. M. Karabo1rk, A. Ersoiz, A. Denizli, R. Say, *Ind. Eng. Chem. Res.* **2008**, *47*, 2258.
22. C. Yu, K.Mosbach, *J. Chromatogr. A* **2000**, *888*, 63.
23. Q. Li, H. J. Su, T. W. Tan, *Biochem. Eng. J.* **2008**, *38*, 212.
24. C. Alexander, H. S. Andersson, L. I. Andersson, R. J. Ansell, N. Krisch, I. A. Nicholls, J. O'Mahony, Whitcombe, M.J. *J. Mol. Recognit.* **2006**, *19*, 106.

25. O. Bruggemann, K. Haupt, L. Ye, E. Yilmaz, K. Mosbach, *J. Chromatogr. A* **2000**, *889*, 15.

26. B. B. Prasad, S. Banerjee, *React. Funct. Polym.* **2003**, *55*, 159.

27. C. Sulitzky, B. Ruckert, A. J. Hall, F. Lanza, K. Unger, B. Sellergren, *Macromolecules* **2002**, *35*, 79.

28. J. Ou, X. Li, S. Feng, J. Dong, X. Dong, L. Kong, M. Ye, H. Zou, *Anal.Chem.* **2007**, *79*, 639.

29. J. Pan, X. Zou, X. Wang, W. Guan, Y. Yan, J. Han, *Chem. Eng. J.* **2010**, *162*, 910.

30. K. Tsukagoshi, K. Y. Yu, M. Maeda, M. Takagi, *Bull. Chem. Soc. Jpn.* **1993**, *66*, 114.

31. Y. M. Ren, M. L. Zhang, D. Zhao, *Desalination* **2008**, *228*, 135.

32. G. H. Wu, Z. Q. Wang, J. Wang, C. Y. He, *Anal. Chim. Acta* **2007**, *582*, 304.

33. X. J. Chang, N. Jiang, H. Zheng, Q. He, Z. Hu, Y. H. Zhai, Y. M. Cui, *Talanta* **2007**, *71*, 38.

34. E. Birlik, A. Ersoz, E. Ac ıkkalp, A. Denizli, R. Say, *J. Hazard. Mater.* **2007**, *140*, 110.

35. N. Candan, N. Tuzmen, M. Andac, C. A. Andac, R. Say, A. Denizli, *Mater. Sci. Eng. C* **2009**, *29*, 144.

36. Y. H. Zhai, Y. W. Liu, X. J.Chang, X. F. Ruan, J. L. Liu, *React. Funct. Polym.* **2008**, *68*, 284.

37. B. Sellergren, C. Sulitzky, B. Ruckert, U.S. Patent 6, **2004**, *488 B1*, 759.

38. F. G. Tamayo, M. M. Titirici, A. M. Esteban, B. Sellergren, *Anal. Chim. Acta* **2005**, *542*, 38.

39. M. Quaglia, E. D. Lorenzi, C. Sulitzky, G. Massoloni, B. Sellergren, *Analyst* **2001**, *126*, 1495.

40. M. Quaglia, E. D. Lorenzi, C. Sulitzky, G. Caccialanza, B. Sellergren, *Electrophoresis* **2003**, *24*, 952.

41. L. Schweitz. *Anal. Chem.* **2002**, *74*, 1192.

42. D. James, G. Venkateswaran, T. P. Rao, *Microporous and Mesoporous Materials* **2009**, *119*, 165.

43. V. Pakade, E. Cukrowska, J. Darkwa, N. Torto, L. Chimuka, Simple and Efficient Ion Imprinted Polymers for Recovery of Uranyl Ion and Chromium (VI) from Environmental Samples, *ANALYTICAL TOOLS AND TECHNIQUES* ,15th ICHMET, 227.

44. S.Y. Bae, G.L. Southard, G.M. Murray, *Analytica Chimica Acta,* **1999,** *397*, 173.

45. F. Caprasse, D. Leroy, L. Martinot, S. Lambert, J. P. Pirard, J. Guillaume, C. Jeromeand R. Jeromed, *J. Mater. Chem.* **2002**, *12*, 137.

46. R. Say, A. Ersoz, A. Denizli, Sep. Sci. Technol. 38 (2003) 3431–3441.

47. W.L. Mock, In Comprehensive Supramolecular Chemistry; Vogtle, Ed.; Pergamon: Oxford, **1996**, *2*, 477.

48. J.W. Lee, S. Samal, N. Selvapalam, H. J. Kim, K. Kim, *Acc. Chem. Res.* **2003**, *36*, 621.

49. J. Lagona, P. Mukhopadhyay, S. Chakrabarti, L. Isaacs, *Angew. Chem. Int. Ed.* **2005**, *44*, 4844.

50. S.D. Choudhury, J. Mohanty, H. Pal, A. C. Bhasikuttan, *J. Am. Chem. Soc.* **2010**, *132*, 1395.

51. K. Kim, *Chem. Soc. Rev.* **2002**, *31*, 96.

52. O. A. Gerasko, D. G. Samsonenko, V. P. Fedin, *Russ. Chem. Rev.* **2002**, *71*, 741.

53. J. X. Lin, J. Lu, H. X. Yang, R. Cao, *Crys. Grow. Des.* **2010**, *10*, 1966.

54. W. A. Freeman, *Acta Crystallogr. Sect. B* **1984**, *40*, 382.

55. H. J. Buschmann, E. Cleve, E. Schollmeyer, *Inorg. Chim. Acta* **1992**, *193*, 93.

56. Y. M. Jeon, J. Kim, D. Whang, K. Kim, *J. Am. Chem. Soc.* **1996**, *118*, 9790.

57. D. Whang, J. Heo, J. H. Park, K. Kim, *Angew. Chem. Int. Ed.* **1998**, *37*, 78.

58. J. Heo, S. Y. Kim, D. Whang, K. Kim, *Angew. Chem. Int. Ed.* **1999**, *38*, 641.

59. J. Heo, J. Kim, D. Whang, K. Kim, *Inorg. Chim. Acta* **2000**, *297*, 307.

60. F. Zhang, T. Yajima, Y. Z. Li, G. Z. Xu, H. L. Chen, Q. T. Liu, O. Yamauchi, *Angew. Chem. Int. Ed.* **2005**, *44*, 3402.

61. J. X. Liu, L. S. Long, R. B. Huang, L. S. Zheng, *Cryst. Growth Des.* **2006**, *6*, 2611.

62. D. G. Samsonenko, J. Lipkowski, O. A. Gerasko, A. V. Virovets, M. N. Sokolov, V. P. Fedin, J. G. Platas, R. Hernandez-Molina, A. Mederos, *Eur. J. Inorg. Chem.* **2002**, *9*, 2380.

63. D. G. Samsonenko, O. A. Gerasko, J. Lipkowski, A. V. Virovets, V. P. Fedin, *Russ. Chem. Bull.* **2002**, *51*, 1915.

64. D. G. Samsonenko, M. N. Sokolov, O. A. Gerasko, A. V. Virovets, J. Lipkowski, D. Fenske, V. P. Fedin, *Russ. Chem. Bull.* **2003**, *52*, 2132.

65. J. X. Liu, L. S. Long, R. B. Huang, L. S. Zheng, *Inorg. Chem.* **2007**, *46*, 10168.

66. O. A. Gerasko, E. A. Mainicheva, M. I. Naumova, O. P. Yurjeva, A. Alberola, C. Vicent, R. Llusar, V. P. Fedin, *Eur. J. Inorg. Chem.* **2008**, *3*, 416.

67. O. A. Gerasko, M. N. Sokolov, V. P. Fedin, *Pure Appl. Chem.* **2004**, *76*, 1633.

68. O. A. Gerasko, D. G. Samsonenko, A. A. Sharonova, A. V. Virovets, J. Lipkowski, V. P. Fedin, *Russ. Chem. Bull.* **2002**, *51*, 346.

69. S. C. Cui, T. Tachikawa, M. Fujitsuka, T. Majima, *J. Phys. Chem. C* **2011**, *115*, 1824.

70. K. Kim, N. Selvapalam, Y. H. Ko, K. M. Park, D. Kim, Kim, *J. Chem. Soc. Rev.* **2007**, *36*, 267.

71. C. A. Burnett, D. Witt, J. C. Fettinger, L. Isaacs, *J. Org. Chem.* **2003**, *68*, 6184.

72. J. Kim, I.-S. Jung, S.-Y. Kim, E. Lee, J. -K. Kang, S. Sakamoto, K. Yamaguchi, K. Kim, *J. Am. Chem. Soc.* **2000**, *122*, 540.

73. P. Thuery, *Cryst. Growth Des.* **2009**, *9*, 1208.

74. P. Thuery, *Cryst. Growth Des.* **2008**, *8*, 4132.

75. J. C. Berthet, M. Nierlich, M. Ephritikhine, *Angew. Chem. Int. Ed.* **2003**, *42*, 1952.

76. *SAINT: Software for the CCD Detector System*; Bruker Analytical X-ray Systems, Inc.: Madison, WI, **1998**.

77. Bruker SADABS, SMART, SAINTPLUS and SHELXTL, Bruker AXS Inc., Madison, WI, USA, **2003**.

78. G.M. Sheldrick, *SHELXS-97, Program for Structure Solution of crystal structure;* University of Gottingen: Germany, **1997**.

79. G.M. Sheldrick, *SHELXL-97, Program for Crystal Structure Analysis;* University of Gottingen: Germany, **1997**.

80. T. Cardinaels, J. Ramaekers, D. Guillon, B. Donnio, K. Binnemans, *J. Am. Chem. Soc.* **2005**, *127*, 17602.

81. Y. Zhang, F. R. Livens, D. Collison, M. Helliwell, F. Heatley, A. K. Powell, S. Wocadlo, Eccles, H. *Polyhedron* **2002**, *21*, 69.

82. Z. Hnatejko, S. Lis, Z. Stryła, Starynowicz, P. *Polyhedron* **2010**, *29*, 2081.

83. Y. Katsumura, H. Abe, T. Yotsuyanagi, K. Ishigure, *J. Photochem. Photobiol., A* **1989**, *50*, 183.

84. E. Rabinowitch, R. L. Belford, *Spectroscopy and Photochemistry of Uranyl Compounds, Pergamon* **1964**, 264.

85. S. J. Formosinho, M. G. Miguel, H. D. Burrows, *J. Chem. Soc., Faraday Trans.* **1984**, *80*, 1717.

86. S. J. Formosinho, H. D. Burrows, M. G. Miguel, M. Emilia, D. G. Azenha, I. M. Saraiva, A. Catarina, D. N. Ribeiro, I. V. Khudyakov, R. G. Gasanov, M. Bolte, M. Sarakha, *Photochem. Photobiol. Sci.* **2003**, *2*, 569.

87. Z. Hnatejko, S. Lis, P. Starynowicz, Z. Stryła, *Polyhedron* **2011**, *30*, 880.

88. S.Y. Jon, N. Selvapalam, D. H. Oh, J. K. Kang, S. Y. Kim, Y. J. Jeon, J. W. Lee, K. Kim, *J. Am. Chem. Soc.* **2003**, *125*, 10186.